Kinetic Study of Olefin Polymerization with a Supported Metallocene Catalyst. I. Ethylene/Propylene Copolymerization in Gas Phase

Z. GENE XU,* S. CHAKRAVARTI, W. HARMON RAY

Department of Chemical Engineering, University of Wisconsin–Madison, Madison, Wisconsin 53706

Received 11 December 1999; accepted 22 January 2000

ABSTRACT: A kinetic study of ethylene homopolymerization and copolymerization is conducted with a supported metallocene catalyst in a gas-phase reactor. An experimental procedure is developed that minimizes the effect of impurities in the reactor and simultaneously yields consistent and reproducible reaction-rate data. The effects of operational parameters such as reaction temperature, pressure, and comonomer concentration on the kinetics of both homopolymerization and copolymerization are investigated. Online perturbation techniques are implemented to determine key kinetic parameters such as the activation energies for ethylene propagation and catalyst deactivation. A reaction-rate order close to 2 is obtained for ethylene homopolymerization from pressure perturbations, while near to first-order dependency is observed in the presence of propylene. To quantify the effects of the operational parameters, a one-site kinetic model for homopolymerization and a two-site kinetic model for copolymerization are proposed. The necessary kinetic parameters in the model are estimated using the POLYRED™ package. The resulting kinetic model represents the kinetic data over a wide range of conditions for this supported metallocene catalyst. © 2001 John Wiley & Sons, Inc. J Appl Polym Sci 80: 81–114, 2001

Key words: ethylene/propylene copolymerization; metallocene catalyst; kinetic study; supported zirconium catalyst; gas phase; parameter estimation

INTRODUCTION

The discovery of Group 4 metallocene–alumoxane systems as catalysts for olefin polymerization has opened up a new frontier in the area of organometallic chemistry and polymer synthesis. The flexibility provided in altering the ligand structure of the catalysts facilitates better control of the architecture of the macromolecule. Some distinct features of the polymers produced by metallocenes are (1) narrower molecular weight distribution,[1] (2) homogeneous comonomer incorporation,[1] and (3) controlled long-chain branching which facilitates better strength and processability properties.[2]

The success of gas-phase processes is testament to the progress attained in the areas of polymerization processes and reactor design.[3,4] Some of the commercial advantages include[5] (i) elimination of costs associated with storage and handling of large amounts of solvent; (ii) simplification of polymerization systems; (iii) fewer environmental concerns due to the absence of the solvent; (iv) flexible production of block copolymers of propylene and ethylene; (v) no monomer or hydrogen solubility concerns; and (vi) no extra costs associated with drying polymers.

Over the years, experimental studies in both academia and industry have been directed toward

Correspondence to: W. H. Ray.
**Current address:* Chemical Division, Goodyear Research and Development, Akron, OH 44303.

Journal of Applied Polymer Science, Vol. 80, 81–114 (2001)
© 2001 John Wiley & Sons, Inc.

gaining a better understanding of supported Ziegler–Natta catalysts in gas-phase reactors for the successful development of LLDPE, HDPE, and EPR processes. In spite of the considerable effort undertaken to integrate metallocene technology into the polymerization processes in the olefin industry, there is a dearth of information on the kinetics of supported metallocene catalysts. From literature reviews,[6–13] no overriding conclusions can be made that generalize the observed kinetics with metallocene catalysts. There are currently only a few detailed studies on the kinetics of metallocenes in liquid-phase reactors[14–22] and even fewer on the performance of supported metallocenes in gas-phase reactors.[1,23]

In general,[24] for transition-metal-catalyzed polymerization, there are three levels of interest: (i) the microscale, where understanding the kinetics is important when discussing effects of types of sites on MWD and copolymer composition; (ii) the mesoscale, where the effects of heat and mass transfer are associated with polymer particle growth; and (iii) the macroscale, which concerns reactor phenomena such as heat removal, residence time distributions, and other factors that influence process control and product transitions in the reactor. So, the main objective of this microscale study was to provide a model that is adequate for continuous reactor design and scale up. The experiments were conducted on supported zirconocenes in a gas-phase stirred-bed reactor system that is capable of controlling the comonomer composition online.[25] The initial emphasis of the investigation involved the determination of an experimental procedure that will produce consistent and reproducible data. Important issues addressed include (i) the operational mode of the reactor, (ii) ability to control operational parameters such as temperature, pressure, and comonomer composition, and (iii) determination of a good scavenging procedure that facilitates high catalyst activity. A detailed study which investigates the effects of reactor pressure, temperature, and comonomer composition on the kinetics of ethylene homopolymerization and ethylene–propylene copolymerization was conducted. Temperature and pressure perturbation techniques were implemented to ascertain important kinetic parameters such as the activation energies of propagation and deactivation and the reaction-rate order with respect to ethylene. Finally, the proposed kinetic model was used to interpret the kinetic data observed under a variety of reaction conditions.

The organization of the paper is as follows: The next section presents the experimental details which include the development of the experimental procedure for studying the kinetic behavior under various reaction conditions. The third section summarizes the kinetic results from the various ethylene homopolymerization and copolymerization experiments. In the fourth section, the parameter estimation results are presented and models are proposed to explain the observed kinetics for ethylene homo- and copolymerization.

EXPERIMENTAL

Reactor System

A lab-scale stirred-bed gas-phase reactor was constructed at the University of Wisconsin Polymerization Reaction Engineering Laboratory (UW-PREL) that facilitates kinetic investigations on Ziegler–Natta and supported metallocene catalysts. Previous studies conducted show that the gas-phase reactor is advantageous for particle growth compared to the slurry reactor where the diluent may extract amorphous material from the polymer particle, thereby affecting postreactor analysis.[26] The current experimental system was originally designed by K.-Y. Choi[27] in 1984 for homopolymerization of ethylene and propylene, subsequently modified by Chen[28] in 1992 for random copolymerization experiments. The system was redesigned and rebuilt by Debling and Han-Adebekun[29] in 1993 for facilitating ethylene copolymerizations with propylene and heavier α-olefins. A detailed description of the reactor system and its various unique features can be found elsewhere.[26,30]

The reactor is a 1-L stainless-steel vessel (manufactured by Parr Instrument Corp.). The reactor support cage permits operation in both the horizontal and vertical modes since a rotation of 90° from the vertical position is possible. Figure 1 depicts the entire reactor system. Figure 2 describes the various ports on the reactor. From Figure 2, it can be noted that use of the U-type stirrer warrants horizontal operation in order to facilitate better particle agitation and heat transfer, which, in turn, avoids particle agglomeration. Gaseous monomers, hydrogen, and nitrogen pass through three stages of purification prior to entering the "monomer injection" port of the reactor. The presence of the thermocouple and pressure transducer facilitate online monitoring of the temperature and pressure during the course of a

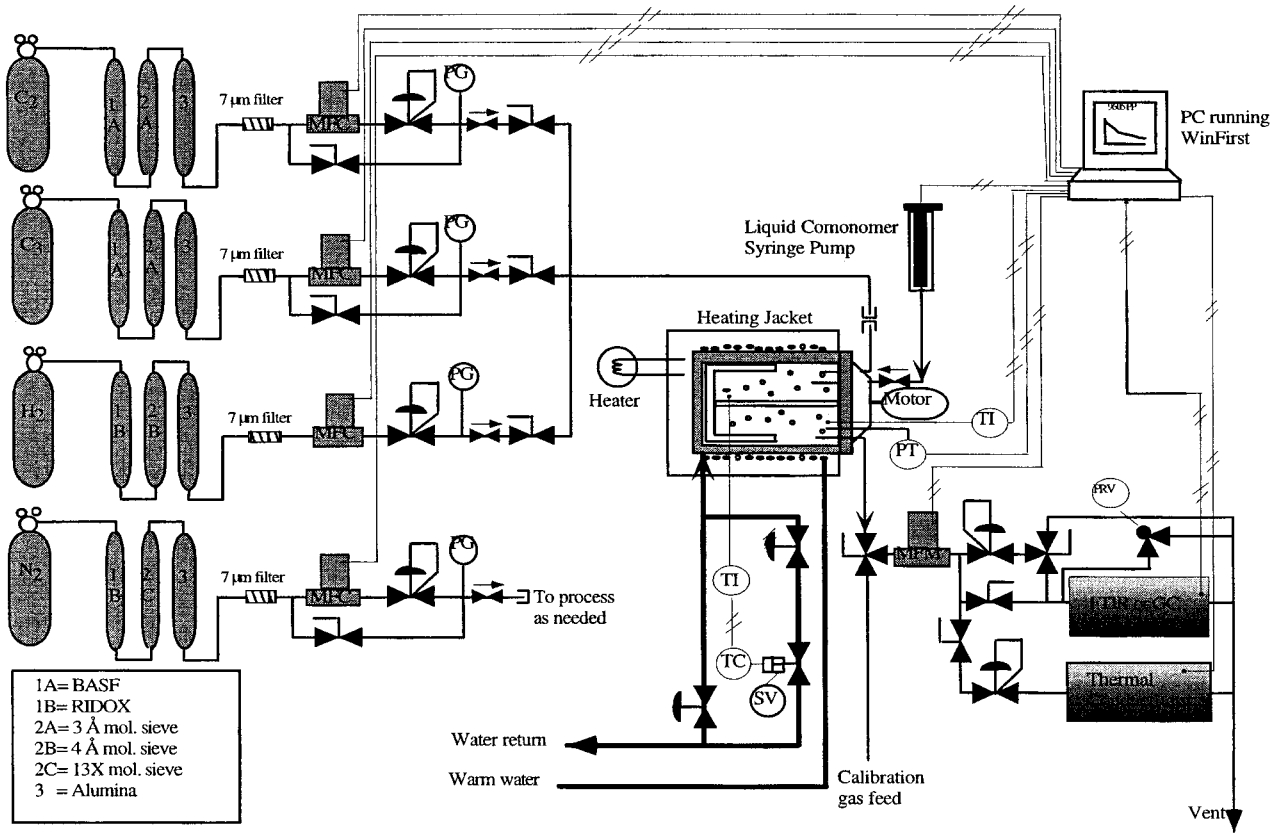

Figure 1 Horizontal stirred bed gas-phase reactor system.

reaction. The syringe pump is used to introduce the liquid comonomer into the reactor. The scavenger and catalyst are injected through different ports on the reactor to avoid possible contamination of the catalyst. The opening or closing of the valve on the "vent" line (see Fig. 2) determines the specific mode of operation of the reactor.

If the valve is closed, the reactor is said to be operating in the "no-purge" mode. In this mode of operation, it is not possible to control the comonomer composition online since there is no exit gas stream entering the FTIR for composition analysis. The pressure in the reactor is maintained by a constant flow of the monomer. This constant flow is used to determine the instantaneous reaction rate of the monomer. Under semibatch operation, the reaction rate is equal to the flow of the monomer into the reactor (assuming negligible accumulation). In the "no-purge" mode, it is not possible to obtain the instantaneous reaction rate for the comonomer. Hence, homopolymerizations are generally conducted in the no-purge mode.

The seed bed is necessary for various reasons: (i) It ensures proper dispersion, (ii) it facilitates better heat transfer between the particles and the reactor wall, and (iii) reliable measurement of the reactor temperature is made possible. Previous studies by Debling[26] showed that Teflon powder (granular resin 9B) proves to be ideal for this purpose. The average seed particle size is 575 μm. The average particle size in the seed bed is further increased by removing particles trapped in a 500-μm sieve. The bed material proved to be gentle enough to avoid any grinding and disintegration of the polymer particles during the experiment.

Efficient control of the reaction temperature and pressure is essential for the success of the experiment. The detailed design of the control system was well documented in the paper by Han-Adebekun et al.[25] A brief description is presented as follows: An on/off controller is used to manipulate the flow rate of the cooling water. Previous studies[25] showed that the temperature can be controlled to well within ± 1°C with a $TiCl_4/MgCl_2$ catalyst.

The reactor pressure is essentially controlled through an upstream or downstream regulator.

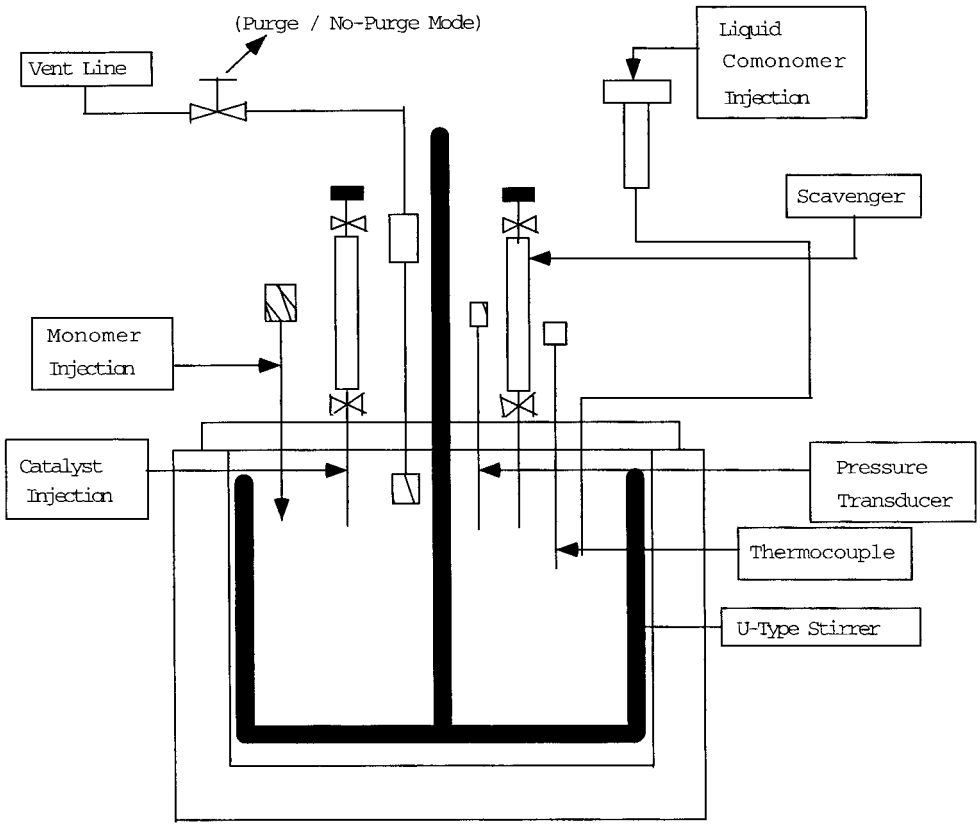

Figure 2 Reactor schematic.

When the reactor is operated in the no-purge mode, the reactor pressure is maintained by the upstream regulator and the monomer flows freely into the reactor. In copolymerization experiments, for the gas-phase composition to be monitored, a continuous gas purge is necessary. For this case, a back-pressure regulator on the purge stream is used to control the pressure in the reactor. A gas flowmeter installed on the purge stream monitors the purge rate.

Effective comonomer composition control is imperative for investigating the kinetics of ethylene copolymerization. A Galaxy 3020 FTIR, purchased from ATI/Mattson Instruments, was used. Debling[26] showed that a step change in propylene composition can be achieved within 2–3 min with the help of a PI controller. In this study, a PI controller with Smith Predictor[31] was employed to adjust the flow rates of the various monomers based upon the data collected from the FTIR.

A scavenging procedure aimed at eliminating the contaminants in the reactor was implemented. The scavenger used is a solution of triethylaluminum (TEA) in sparged heptane. A separate port on the reactor is used to inject the TEA solution to prevent possible contamination of the catalyst. The catalyst used in this work was an unbridged zirconocene supported together with MAO on silica.

Experimental Procedure

Due to the highly sensitive nature of the catalyst used in this work, care must be taken in handling the catalyst and preparing the reactor in order to obtain reliable kinetic data. The following experimental procedure was implemented:

- Day before the reaction

  1. The seed bed is loaded into the reactor (the seed bed was stored in an oven at about 60°C for over 24 h). The reactor is pressurized overnight to determine the presence of leaks in the reactor.

- Day of the reaction

  1. Reactor preparation: To maintain an inert atmosphere with low levels of impurities

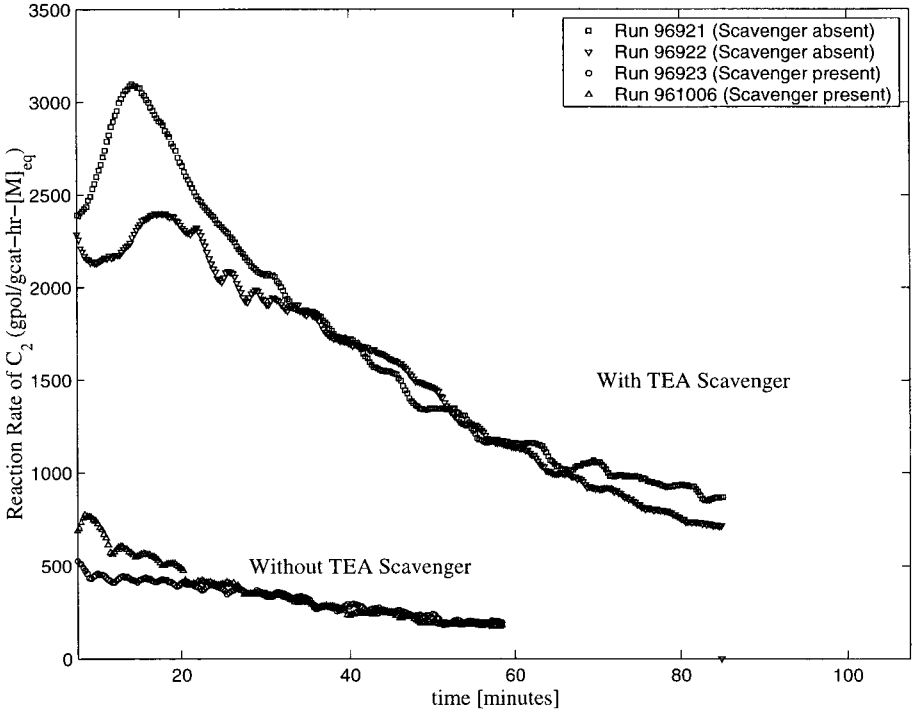

Figure 3 Comparison of reaction-rate curves for ethylene homopolymerization with/without scavenger.

such as moisture and oxygen, the reactor is subjected to 2 h of heat evacuation and 1 h of purging with ultrahigh pure (UHP) nitrogen at a temperature between 60 and 70°C.

2. Scavenging procedure: The purging is followed by the scavenging procedure which involves injecting the scavenger (a solution of TEA in heptane) and pressurizing the reactor. This lasts for 15 min.
3. This is followed by a UHP nitrogen purge for about 45 min to remove the scavenger prior to catalyst injection.
4. Catalyst injection: The catalyst is typically injected at about 5–7°C below the reaction temperature.
5. Starting the reaction: Following the catalyst injection, the temperature is then increased to the reaction temperature as the monomers are introduced simultaneously.

No-purge Mode Operation

Ethylene homopolymerization is carried out to determine the effect of a scavenging procedure. Kinetic profiles obtained from ethylene homopolymerizations conducted in the presence and absence of a scavenger are shown in Figure 3. It is observed that the curves are fairly reproducible and exhibit decay-type kinetics.[32]

The lowering of the catalyst activity in the absence of scavenger is attributed to the presence of trace amounts of impurities such as oxygen and moisture in the reactor. Since the scavenging procedure needs to be effective, an optimum level needs to be determined such that the TEA does not switch roles from that of a scavenger to that of a poison.[33] Studies[34] have shown that 1.5 cc of TEA [solution of TEA (10%) in heptane] in conjunction with a scavenging time of about 15 min provides a good scavenging procedure that facilitates good catalyst activity.

Although impurities can be significantly reduced by the introduction of TEA, accumulation of impurities will, nevertheless, occur when the reactor is operated in the no-purge mode. It was reported that hydrogen could be produced in reactions with metallocene catalysts.[1] The presence of such species could change the nature of the observed kinetics. A way to minimize these effects in the current reactor system is through purge-mode operation under which a constant flow of the monomer purges the reactor and keeps the concentration of the various other species at low levels.

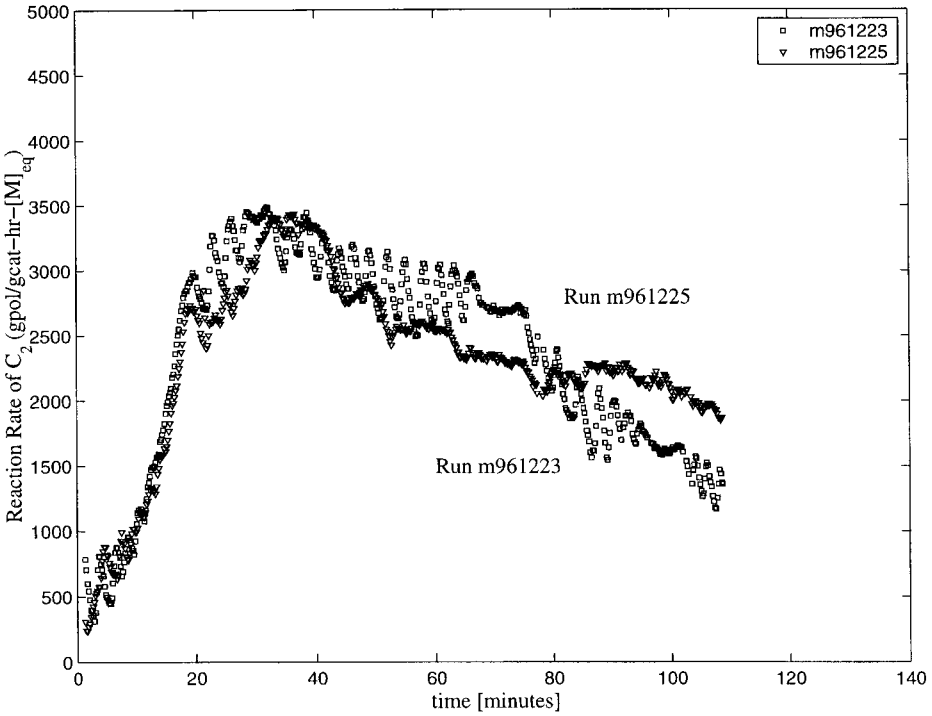

Figure 4 Comparison of copolymerization runs in the purge mode; ethylene/propylene: 0.95/0.05.

Purge-mode Operation

Ethylene–propylene copolymerization conducted under purge-mode operation is shown in Figure 4. When compared to ethylene homopolymerization (conducted in the no-purge mode), an increase in activity and improvement in reproducibility can be observed. In addition, there is a delay in the appearance of the peak for copolymerization, compared to homopolymerization. The control of the operational parameters of temperature, pressure, and composition for the entire duration of the reaction is illustrated in Figure 5. Apart from the first few minutes, the temperature can indeed be controlled to within ± 0.5°C for the entire reaction time. The comonomer composition reaches the expected level of concentration within a short period of time and is effectively controlled at this set point for the entire duration of the reaction. To summarize the observations made from the purge-mode experiments on ethylene–propylene copolymerization: (i) The catalyst displays decay-type kinetics; (ii) the decay rate is less severe compared to that observed with ethylene homopolymerization; and (iii) the procedure provides reproducible data and efficient control of operational parameters.

KINETICS OF ETHYLENE HOMO- AND COPOLYMERIZATION

Experimental Kinetic Results

Table I summarizes the various operating conditions. They are identified by a combination of letters and digits according to propylene gas-phase composition and reaction temperature. For instance, EP-10P-62C would correspond to ethylene/propylene copolymerization with 10 mol % propylene in the gas phase and a reaction temperature of 62°C. For ethylene homopolymerization, the label HDPE is assigned to distinguish this from the copolymers being produced.

All the experiments were performed with the reactor operating in the purge mode. Note that the catalyst used in the following studies is from a different batch as compared to the one used in the determination of the experimental procedure.

Ethylene Homopolymerization

The twin issues of concern while considering temperature effects in ethylene homopolymerization are (i) the magnitude of the reaction rate peak and (ii) the location of the peak. This reflects the extent to which the change in reaction tempera-

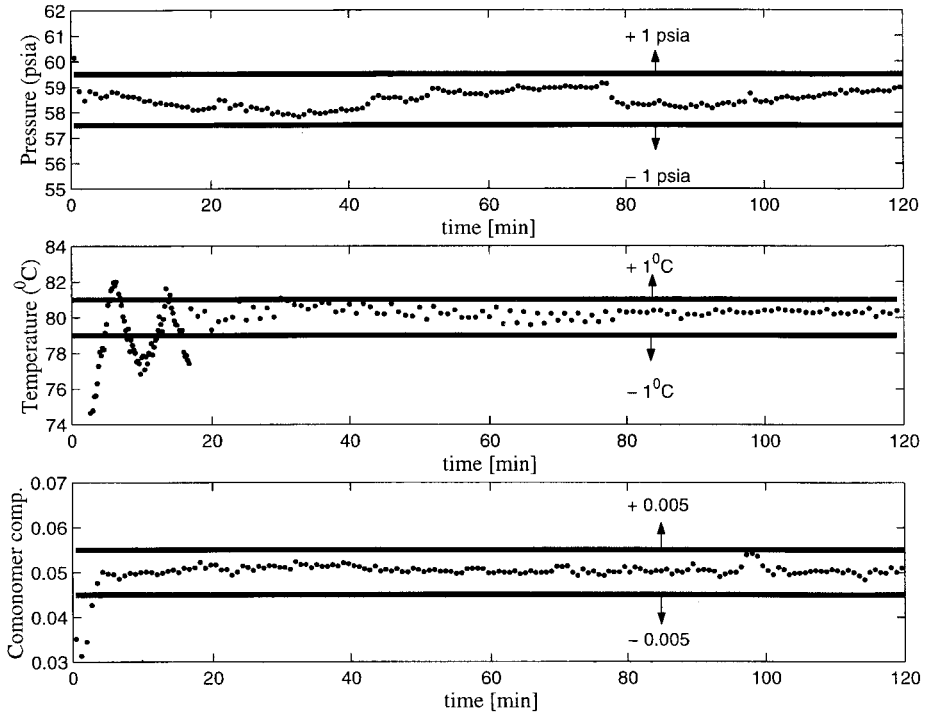

Figure 5 Pressure, temperature, and comonomer composition control.

ture affects the buildup period and decay rate. Previous studies conducted with conventional Ziegler–Natta catalysts showed that the peak value is attained almost instantaneously[26,28,30] at industrial operating temperatures. The emphasis of the few studies[35–37] with unsupported metallocenes was directed toward investigating the effect of temperature on productivity, catalyst activity, and polymer properties. For the present supported catalyst, reaction-rate profiles ob-

Table I Summary of Experimental Runs

Run	C2 in Gas	C3 in Gas	Total Pressure (psia)	Temperature (°C)
		Ethylene Homopolymerization		
HDPE-62C[a]	1.0	—	71	70
HDPE-70C[a]	1.0	—	71	70
HDPE-80C[a]	1.0	—	71	70
		Ethylene Copolymerization		
EP-05P-62C[a]	0.95	0.05	71	62
EP-05P-70C[a]	0.95	0.05	71	70
EP-05P-80C[a]	0.95	0.05	71	80
EP-10P-62C[a]	0.90	0.10	71	62
EP-10P-70C[a]	0.90	0.10	71	70
EP-10P-80C	0.90	0.10	71	80
EP-20P-62C[a]	0.80	0.20	71	62
EP-20P-70C[a]	0.80	0.20	71	70
EP-20P-80C	0.80	0.20	71	80
EP-30P-62C	0.70	0.30	71	62
EP-30P-70C	0.70	0.30	71	70
EP-30P-80C	0.70	0.30	71	80

[a] Used in parameter estimation in the section Parameter Estimation and Model Building.

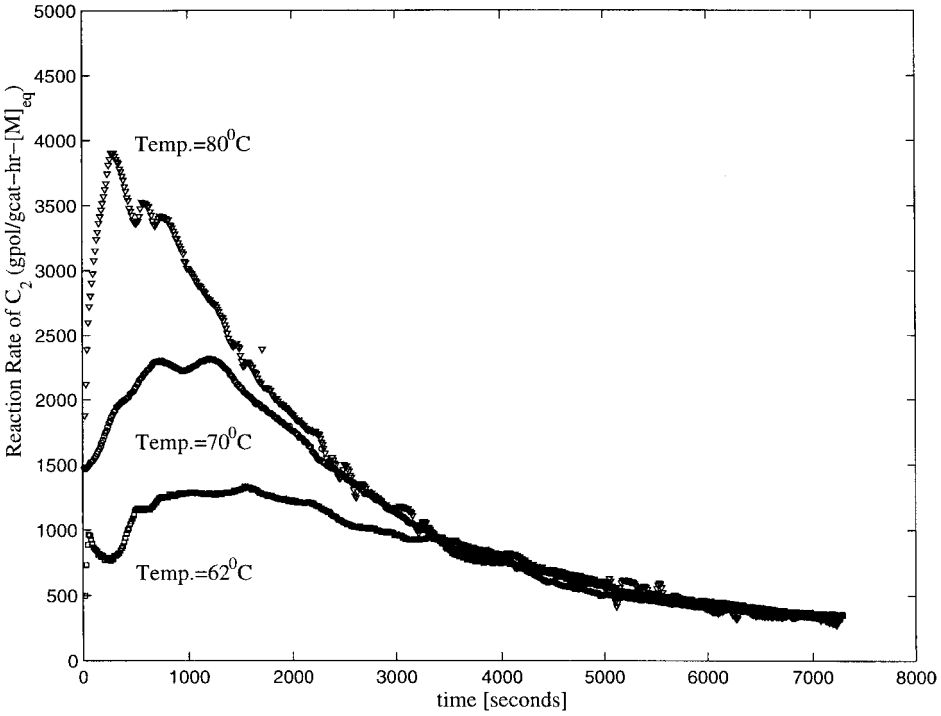

Figure 6 Influence of temperature on ethylene homopolymerization kinetics; $P = 71$ psia.

tained at a reaction pressure of 71 psia with changing temperature are shown in Figure 6. With an increase in reaction temperature, the magnitude of the peak increases and the position of the peak seems to have advanced. However, initial reactor temperature profiles can influence this result. A plot of the temperature profiles for each of the experiments is shown in Figure 7. In general, there is an induction time to increase the temperature of the reactor to the specified level. This exists since the catalyst is typically injected at a slightly lower temperature. In the case of the experiment conducted at 80°C, this induction time is much shorter, which would provide an explanation for the earlier appearance of the peak compared to the other runs. It should be noted that the temperature is well controlled with minor fluctuations around the set point in all the experimental runs.

Ethylene Copolymerization

Figures 8–14 depict the observed comonomer concentration and temperature effects in ethylene–propylene copolymerization kinetics. Figures 15–17 present the reactor temperature profiles under the various copolymerization conditions. An induction time (which is not the same for each run) is present in all the reactor temperature profiles. This induction time has to be accounted for while interpreting the observed rate of activation and reaction-rate peak location.

- Effect of comonomer: At a temperature of 62°C, increasing the comonomer concentration tends to increase the intrinsic ethylene reaction rate (see Fig. 8). This trend is not as pronounced at 70°C; although there is a large increase from the homopolymerization case, a further increase in comonomer concentration causes a hardly noticeable increase in the ethylene reaction rate (see Fig. 9). At 80°C, a similar behavior is observed except that a decrease in the ethylene reaction rate is seen at a comonomer level of 30% (see Fig. 10). On completion of the runs at 80°C, the polymer obtained was found to be quite sticky. This could be attributed to the onset of polymer sintering for the higher propylene content runs. Despite the variation in induction times required to reach the reactor set-point temperature for the different reaction conditions, there is an obvious shift in the reaction peak position for copolymerization when compared to homopolymerization. Looking at the data, it is not easy to provide

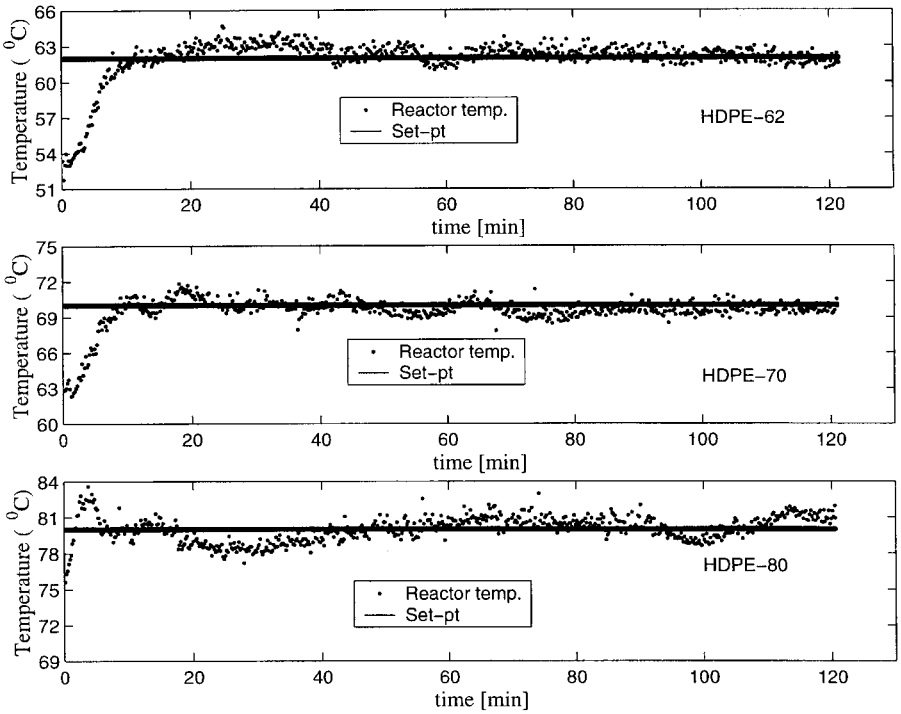

Figure 7 Temperature profiles obtained under the different reaction conditions for ethylene homopolymerization.

a unique interpretation for the observed comonomer effects. The observations of the "comonomer effect" can be consistent with a site-activation mechanism, because for the lower temperature with slower site activation, increasing comonomer concentrations

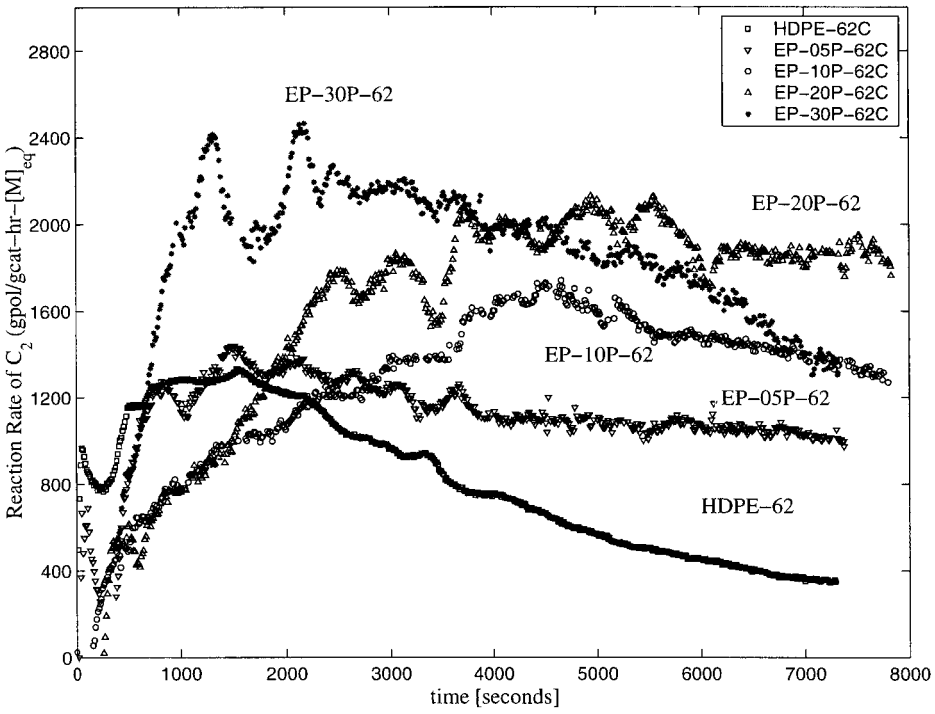

Figure 8 Changing kinetic profiles with comonomer concentration at 62°C.

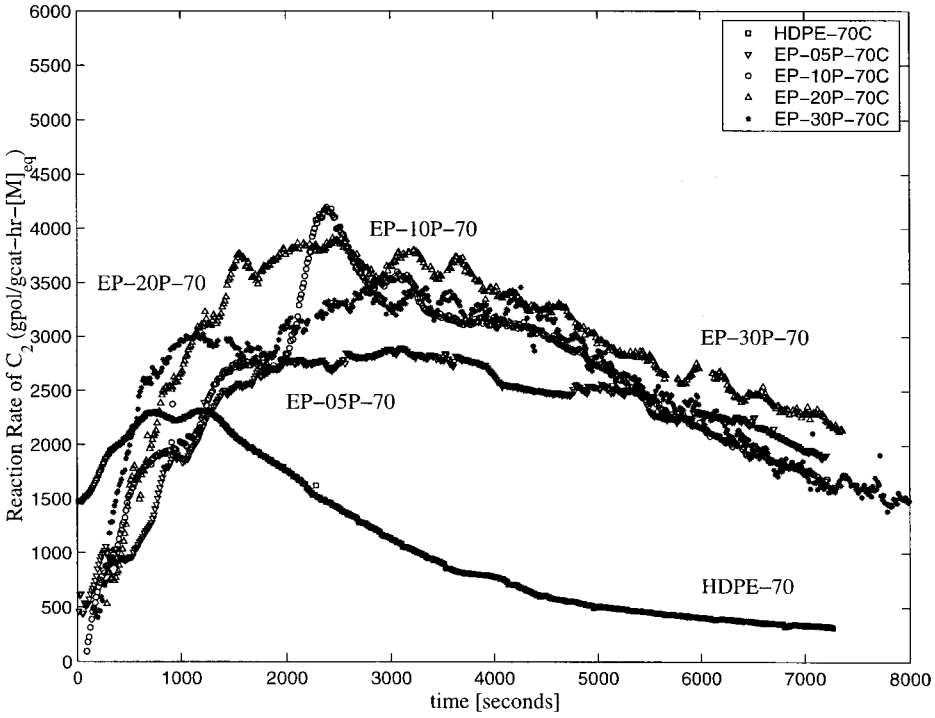

Figure 9 Changing kinetic profiles with comonomer concentration at 70°C.

enhance the rate; however, for intrinsically rapid activation at higher temperatures, only the presence of the comonomer is required to see the increased reaction rate. Alternatively, the enhanced reaction rate observed in the presence of the comonomer could be

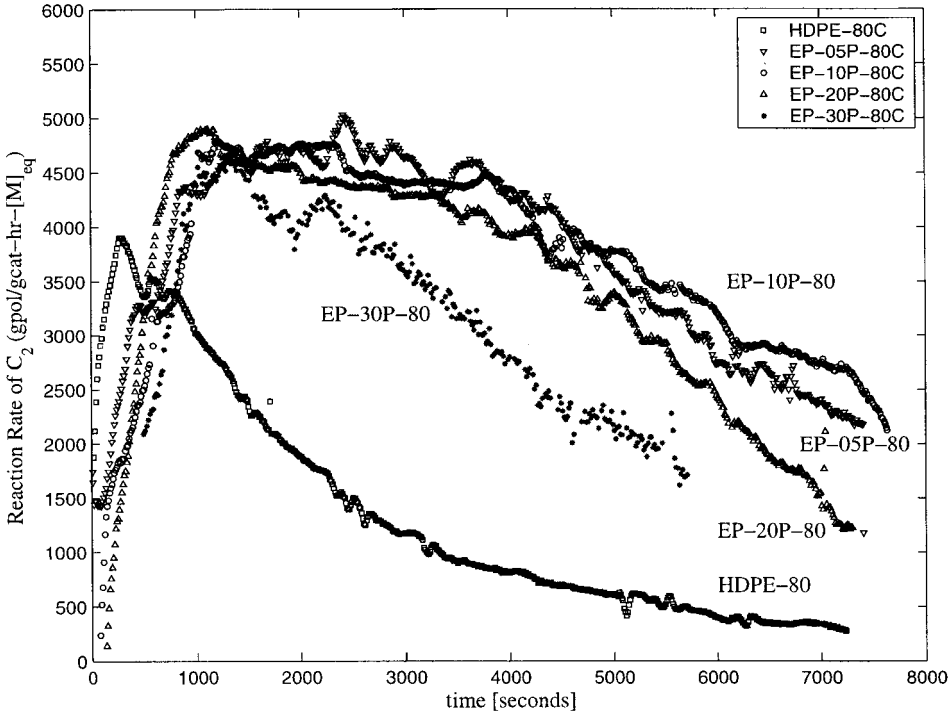

Figure 10 Changing kinetic profiles with comonomer concentration at 80°C.

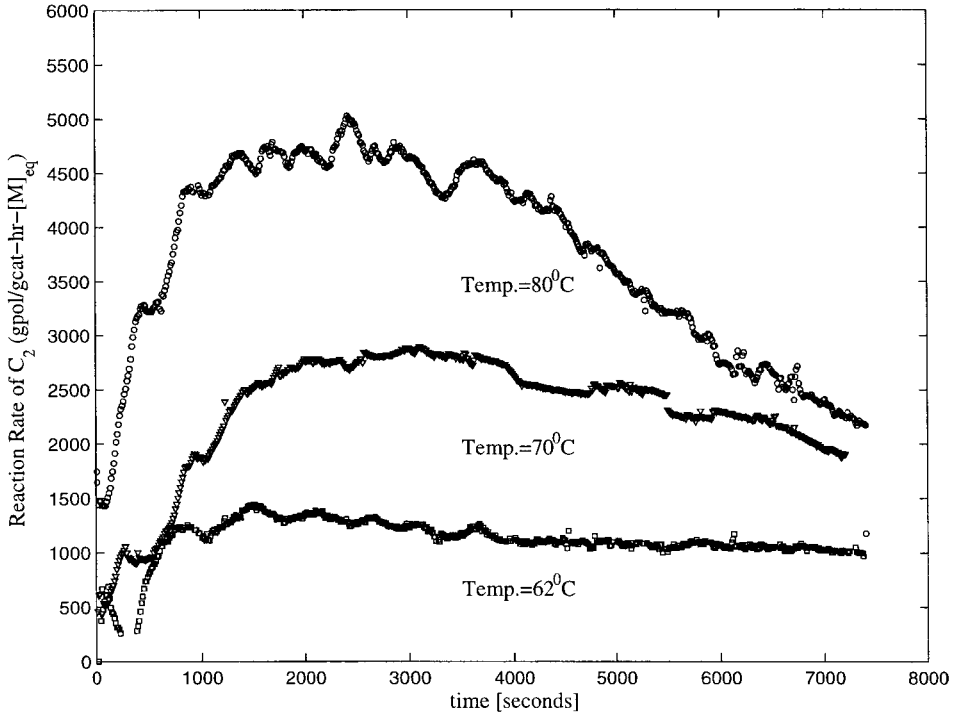

Figure 11 Changing kinetic profiles with temperature at a comonomer concentration of 5%.

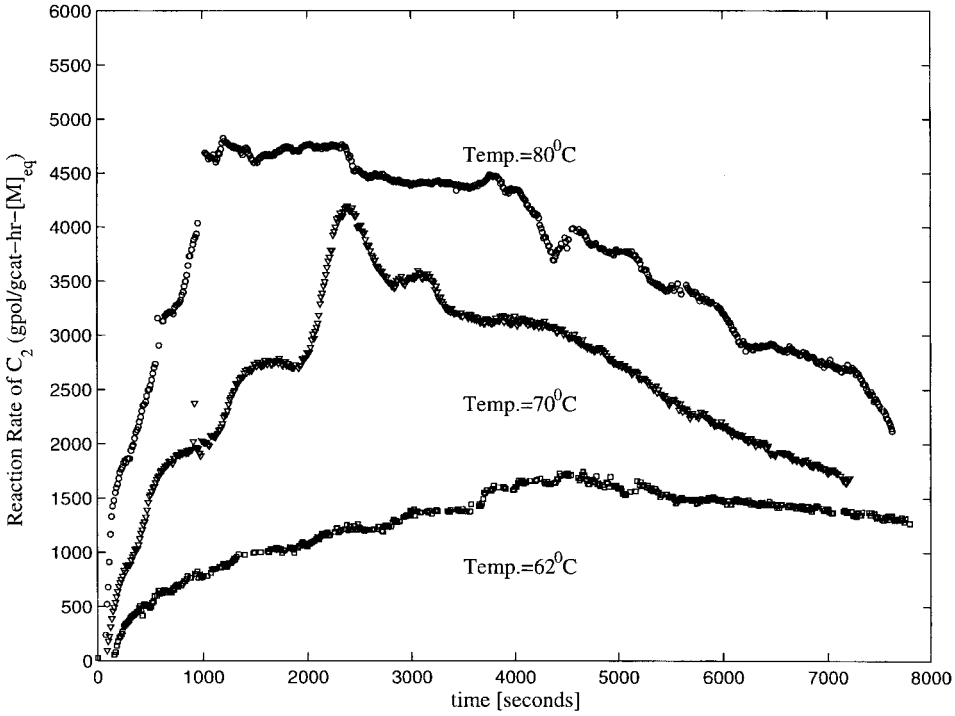

Figure 12 Changing kinetic profiles with temperature at a comonomer concentration of 10%.

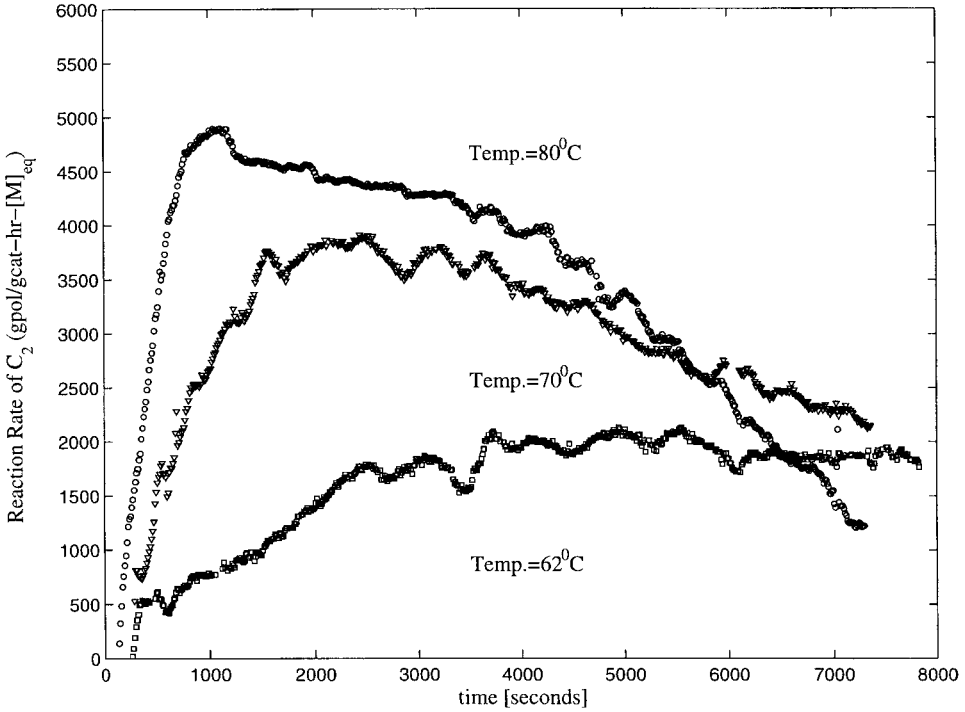

Figure 13 Changing kinetic profiles with temperature at a comonomer concentration of 20%.

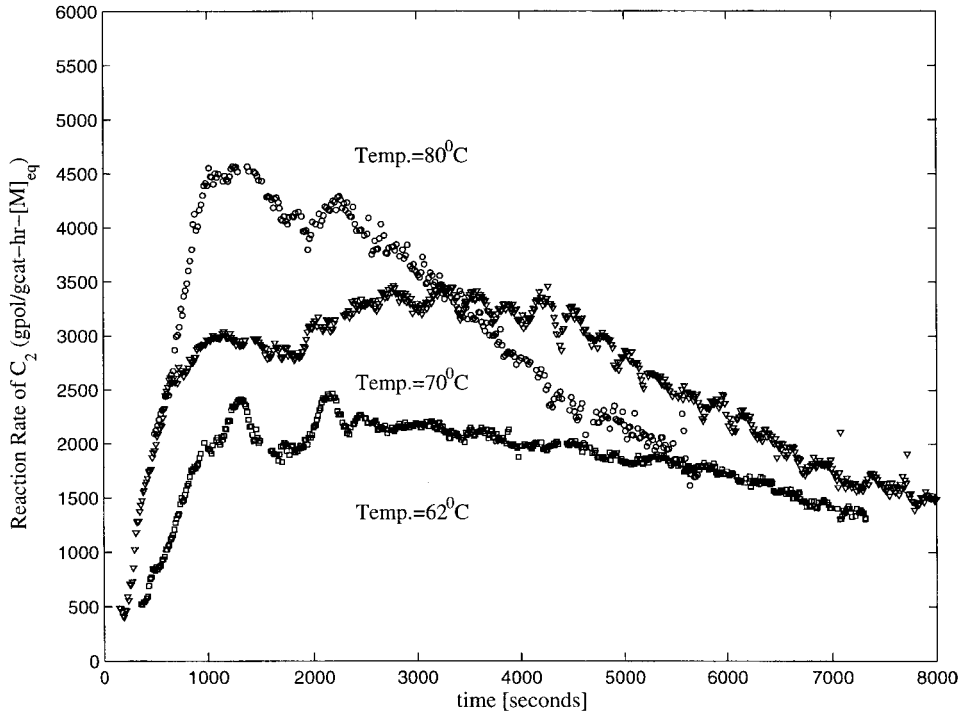

Figure 14 Changing kinetic profiles with temperature at a comonomer concentration of 30%.

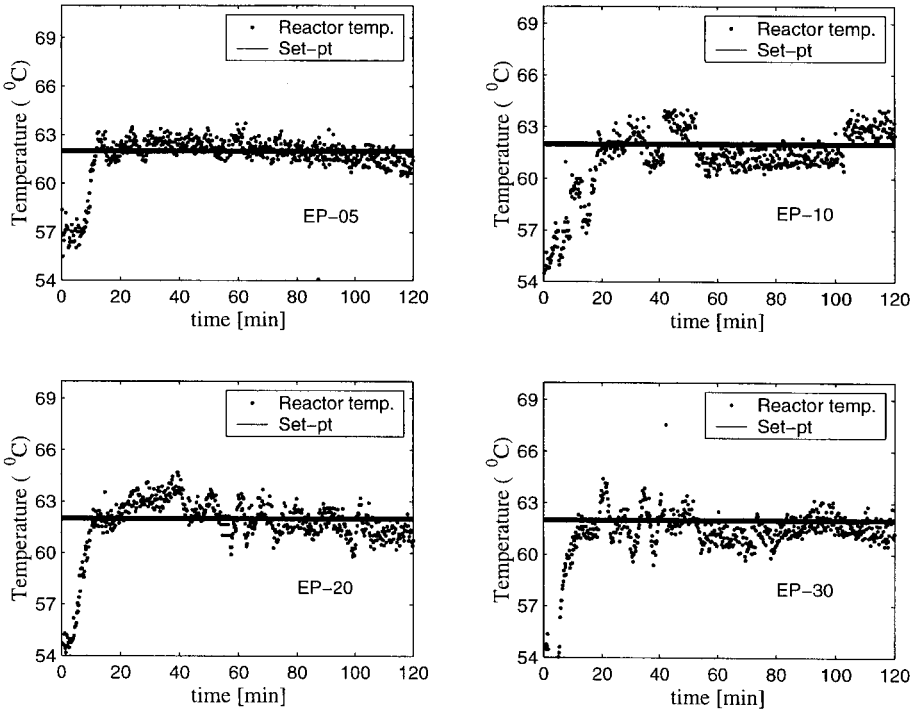

Figure 15 Reactor temperature profiles; set point: 62°C.

attributed to the comonomer stabilizing the sites activated by ethylene, thereby slowing deactivation.

- Temperature effects: The temperature effects on the kinetics are shown in Figures 11–14. From the temperature profiles shown

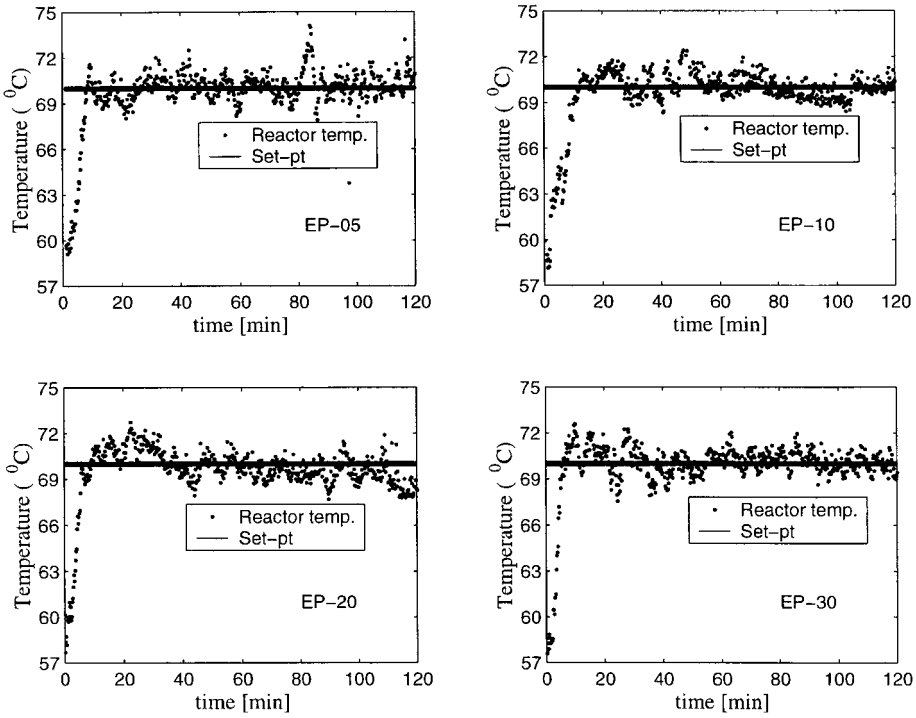

Figure 16 Reactor temperature profiles; set point: 70°C.

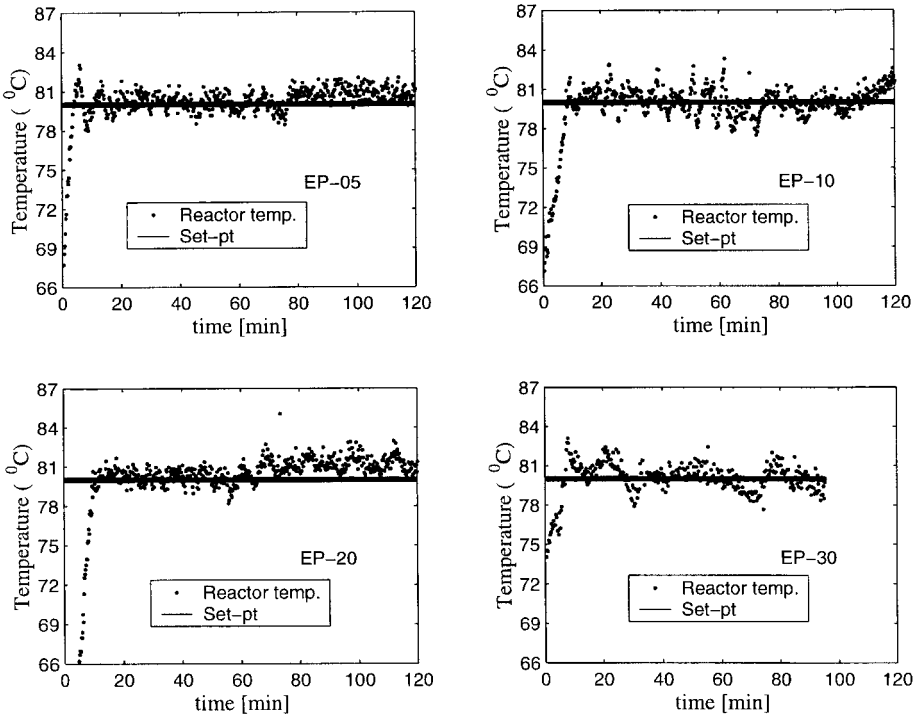

Figure 17 Reactor temperature profiles; set point: 80°C.

in Figures 15–17, it is noted that a variation exists in the initial temperature induction times for each experimental run. Hence, it is not possible to categorically state any general trend about changing peak positions with an increase in the reaction temperature. However, as the temperature increases, the magnitude of the reaction-rate peak increases and catalyst decay becomes more rapid.

PARAMETER ESTIMATION AND MODEL BUILDING

Estimation of Kinetic Parameters via Online Perturbation

In catalyzed olefin polymerization, online perturbation techniques have been employed to characterize the catalytic behavior by investigating issues related to site activation, propagation, and deactivation.[26,30,38] The extent to which these strategies can be implemented is highly dependent on the catalyst and the reactor system. In the current gas-phase reactor system, a variety of perturbation techniques (such as step, pulse, and ramp)[26,30] were effectively implemented to extract several key kinetic parameters. With a supported $TiCl_4/MgCl_2$ catalyst, Hamba et al.[39] were successful in estimating activation energies for catalyst deactivation and monomer propagation through a temperature pulse technique. Debling[26] also estimated activation energies for catalyst deactivation and monomer propagation via step-perturbation techniques.

In this study, the kinetics of ethylene homopolymerization and ethylene–propylene copolymerization with a supported metallocene catalyst were investigated. From the previous section, it was observed that the catalyst behavior is predominantly characterized by decay-type kinetics. The characteristics of the reaction-rate profile depend on the reaction temperature and comonomer composition in the gas phase. The online perturbations in this study were initiated following the appearance of the reaction-rate peak. Table II summarizes the operating conditions for the set of perturbation experiments: Different copolymerization conditions were studied, namely, HDPE (ethylene homopolymerization) and EP (ethylene copolymerization with 5, 10, and 20% propylene in the gas phase).

Data Analysis from Perturbation

Three perturbation techniques: step-up, step-down, and pulse, were employed in this study.

Table II Reaction Conditions for Online Perturbations

	HDPE	EP-5P	EP-10P	EP-20P
		Temperature Perturbation		
Total pressure (psia)	71	71	71	71
C_3 in gas	—	5%(mol)	10% (mol)	20% (mol)
		Pressure Perturbation		
Reactor temperature (°C)	70	70	70	—
C_3 in gas	—	5%(mol)	10% (mol)	—

The step-up and step-down techniques involve raising/lowering an operational parameter incrementally over a period of reaction time. Pulse perturbation was implemented only for the reaction temperature in this work. The interested reader is referred to the article by Hamba et al.[39] for a complete description of these different perturbation techniques.

Since the online perturbations are always applied after the appearance of the rate peak, the reaction rates resulting from the perturbations typically decrease monotonically. A one-site model with first-order decay is selected to describe the observed reaction rates. If there is more than one site, the parameters obtained will be assumed to be average values. For homopolymerization, the monomer consumption rate can be described as

$$Rp\left[\frac{\text{gpol}}{\text{gCat, h}}\right] = Ak_pC^*[M]_{\text{eq}} \tag{1}$$

where $[M]_{\text{eq}}$ [=] (mol/L-amorphous polym.) is the monomer concentration at the catalyst site, k_p [=] (cc-amorphous polym./mol-act.sites.s), C^* [=] (mol-act.sites/gCat), and A (conversion factor) = MW $*$ 3600/1000. The monomer concentration may relate to the pressure of the species, P_i by the following equation:

$$[M]_{\text{eq}} = k_i^* P_i \tag{2}$$

where k^* is the Henry's law constant and is determined by Stein's correlation[40]:

$$\log(k_i^*) = -2.38 + 1.08\left(\frac{T_{c_i}}{T}\right)^2$$

where T_{c_i} is the critical temperature of species i and T is the reaction temperature.

Since the reaction rate calculated from eq. (1) is dependent on the particular reaction conditions, a normalized rate is necessary to facilitate the comparison at different conditions. In this study, the kinetic data is presented as the polymerization rate of monomers (ethylene or propylene): (gPolymer)/(gCat, h, $[M_i]_{\text{eq}}$), that is, it has been normalized by the monomer concentration in the amorphous polymer ($[M_i]_{\text{eq}}$). Based on the units used, it should be noted that the intrinsic reaction rate will depend on the monomer concentration only if the reaction-rate order with respect to the particular monomer is different from 1.

The copolymerization rate expression is derived from the following equations:

$$P_{n,1} + M_1 \xrightarrow{k_{p11}} P_{n+1,1}$$

$$P_{n,1} + M_2 \xrightarrow{k_{p12}} P_{n+1,2}$$

$$P_{n,2} + M_1 \xrightarrow{k_{p21}} P_{n+1,1}$$

$$P_{n,2} + M_2 \xrightarrow{k_{p22}} P_{n+1,2}$$

The monomer consumption rates during copolymerization are

$$Rp\left[\frac{\text{g } M_1 \text{ converted}}{\text{gCat, h}}\right] = Ak_{p,11}C_1^*\beta_1[M_1]_{\text{eq}} \tag{3}$$

$$Rp\left[\frac{\text{g } M_2 \text{ converted}}{\text{gCat, h}}\right] = Ak_{p,22}C_2^*\beta_2[M_2]_{\text{eq}} \tag{4}$$

$$\frac{dC^*}{dt} = -k_dC^*t \tag{5}$$

where 1 and 2 correspond to ethylene and propylene, respectively. C_i^* denotes the concentration of active sites with end group i. C^* ($= \Sigma_i C_i^*$) is the total concentration of active sites. Parameters β_1 and β_2 are defined as

$$\beta_1 = 1 + \frac{1}{r_1}\frac{[M_2]_{eq}}{[M_1]_{eq}} \tag{6}$$

$$\beta_2 = 1 + \frac{1}{r_2}\frac{[M_1]_{eq}}{[M_2]_{eq}} \tag{7}$$

Here, r_1 and r_2 are reactivity ratios:

$$r_1 = \frac{k_{p,11}}{k_{p,12}} \qquad r_2 = \frac{k_{p,22}}{k_{p,21}} \tag{8}$$

In arriving at the expressions of β_1 and β_2, the following quasi-steady-state assumption was used:

$$k_{p,12}C_1^*[M_2]_{eq} = k_{p,21}C_2^*[M_1]_{eq} \tag{9}$$

It will be shown that the reactivity ratios, r_1 and r_2, are not strong functions of temperature; thereby, β_1 and β_2 are also weak functions of temperature.

To extract the kinetic parameters from the online temperature perturbation data, the effects of equilibrium monomer concentration shifts (due to changes in reaction temperature) need to be removed. The intrinsic homopolymerization rates for monomers are therefore used and are defined as follows:

$$Rp_{\overline{kin}}(M_1)\left[\frac{\text{g } M_1 \text{ converted}}{\text{g Cat h mol/L}}\right] = \frac{Rp(M_1)}{\beta_1[M_1]_{eq}} \tag{10}$$

$$Rp_{\overline{kin}}(M_2)\left[\frac{\text{g } M_2 \text{ converted}}{\text{g Cat h mol/L}}\right] = \frac{Rp(M_2)}{\beta_2[M_2]_{eq}} \tag{11}$$

In this study, the comonomer (propylene) reaction rate was found to be extremely low, so the focus is on monomer 1: ethylene. The ethylene intrinsic kinetic rate is used to analyze the data from the online perturbations.

Without loss of generality, the following data analysis is applied to the results from the temperature perturbation. The focus is on the correction of reaction rates due to catalyst deactivation. Because of catalyst deactivation, an increase in temperature may not be associated with an expected increase in the reaction rate. Hence, an appropriate method to correct for catalyst decay is necessary and is summarized.

The correction procedure consists of two steps: The first step involves correcting the reaction rate within an interval in which the temperature is held constant. The second step is to correct the reaction rate between the perturbations. To illustrate the concept, let us consider the tutorial example in Figure 18 in which the reaction-rate response is sketched for an applied temperature perturbation. The reaction rate at time $t_{2,i}$ in the second interval is

$$Rp_{\overline{2,i}} = Ak_{p,11}C_1^*(T_2, t_{2,i}) \tag{12}$$

To correct this reaction rate, the following steps are taken: The first step is to correct within the interval. In the rate expression (12), the kinetic rate constant $k_{p,11}$ is a function of temperature. Once the temperature is kept constant, $k_{p,11}$ remains a constant. If there was no catalyst deactivation, the reaction rate would be constant within the temperature interval. However, deactivation is one of the characteristics of catalysts. To account for the effect due to the catalyst deactivation, a correction factor, f_d^2, is introduced and defined as

$$f_d^2(t_{2,i} - t_{2,\text{ref}}) = \frac{C_1^*(T_2, t_{2,i})}{C_1^*(T_2, t_{2,\text{ref}})} \tag{13}$$

where $t_{2,\text{ref}}$ is the reference point in the interval. For simplicity, the onset of the perturbation is chosen as the reference point in this study (i.e., $t_{2,\text{ref}} = t_{2,s}$). Since first-order deactivation is assumed in this work, $f_d^2(t_{2,i} - t_{2,s})$ can be found to be

$$f_d^2(t_{2,i} - t_{2,s}) = \frac{1}{e^{-k_d(T_2)(t_{2,i} - t_{2,s})}} \tag{14}$$

The next step involves the correction of the reaction rate during the transition time between the temperature perturbations (i.e., time from $t_{1,e}$ to $t_{2,s}$). It normally takes a few minutes for the reactor temperature to reach a new level since it is dependent on the supply of power to the heating jacket on the reactor. The dynamics of the site deactivation during this transition time can be theoretically described by

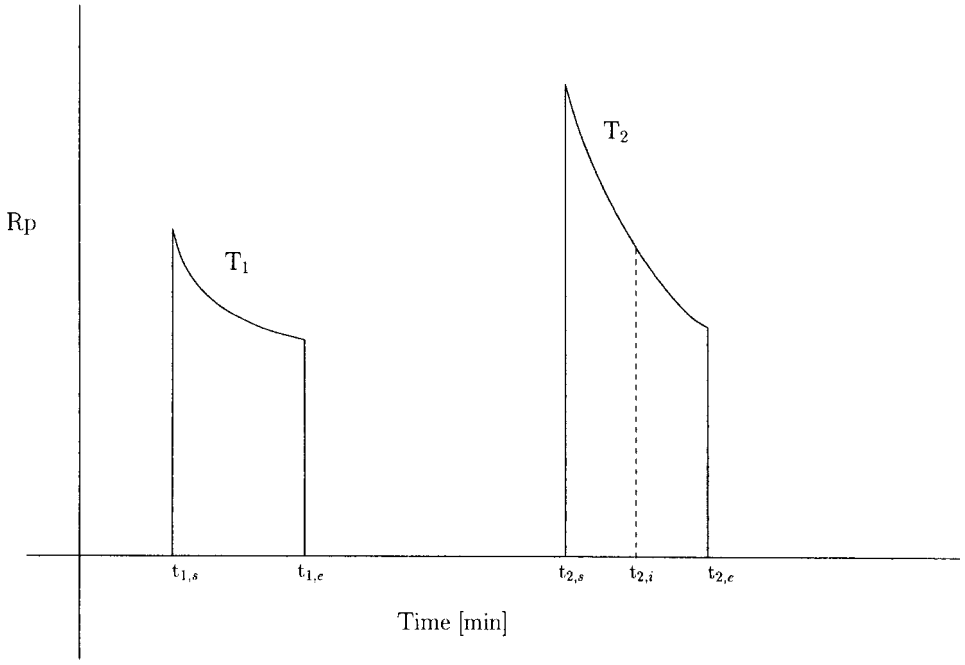

Figure 18 Reaction-rate correction procedure for temperature perturbation. Two temperature intervals are shown. The subscripts "s" and "e" stand for the start and end of the perturbation period, respectively.

$$C_1^*(T_2,\, t_{2,s}) = C_1^*(T_1,\, t_{1,e})\exp[-\int_{t_{1,e}}^{t_{2,s}} k_d(T(t))\, dt]\phi(T_2 - T_1) \tag{15}$$

where function ϕ is related to the sites activated by the temperature and so is a function of temperature. The exact relationship of temperature with time is recorded during the run. The net loss of the active sites during the temperature transition can be estimated as

$$f_d^{1\to 2} = \frac{C_1^*(T_2,\, t_{2,s})}{C_1^*(T_1,\, t_{1,e})} = \exp[-\int_{t_{1,e}}^{t_{2,s}} k_d(T(t))\, dt]\phi(T_2 - T_1) \tag{16}$$

If the onset of the first perturbation is chosen to be the reference point (i.e., $t_{1,s}$), the net loss of the catalyst active sites from point $t_{1,s}$ to $t_{2,i}$ will be

$$f_d^1(t_{1,e} - t_{1,s}) f_d^{1\to 2} f_d^2(t_{2,i} - t_{2,s}) \tag{17}$$

Therefore, the corrected reaction rate at $t_{2,i}$ is

$$Rp_{2,i}^{\text{corr}} = \frac{Ak_p(T_2)C_1^*(T_2,\, t_{2,i})}{f_d^1(t_{1,e} - t_{1,s}) f_d^{1\to 2} f_d^2(t_{2,i} - t_{2,s})} \tag{18}$$

A general expression for the corrected reaction rate at time i in the n^{th} temperature interval can be written as

$$Rp_{n,i}^{\text{corr}} = \frac{Ak_p(T_n)C_1^*(T_n,\, t_{n,i})}{\prod_{j=1}^{n-1} f_d^j(t_{j,e} - t_{j,s}) f_d^{j\to j+1} f_d^{j+1}(t_{n,i} - t_{n,s})} \tag{19}$$

After the correction, the reaction rate at different times within one temperature interval should be identical assuming that there are no monomer diffusion limitations. Figure 19 shows an example of the corrected ethylene reaction rate during temperature step increase. It supports our analysis and also indicates that the temperature is controlled reasonably well.

The data analysis from an online pulse temperature perturbation is slightly different from those for the step-up and step-down experi-

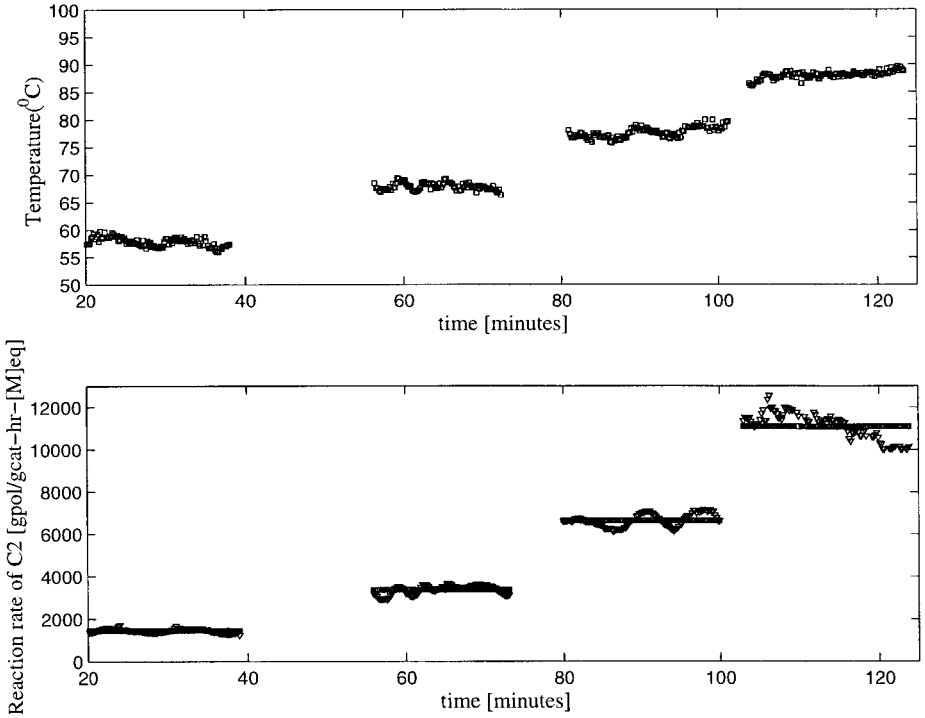

Figure 19 Corrected reaction rate during temperature-step increase.

ments. The detailed derivation was presented by Hamba et al.[39]

Kinetic Parameters

In this section, the kinetic parameters obtained from our temperature and pressure perturbation techniques are presented. Three online perturbation techniques were used in this study: step-up, step-down, and pulse. Step-up and step-down of temperature and pressure perturbations were implemented. A pulse temperature perturbation was also implemented.

Catalyst Deactivation and Monomer Propagation—Homopolymerization

It was observed that the kinetic behavior of ethylene homopolymerization is different from that of copolymerization. To quantify this difference, a set of perturbation techniques was employed to determine the activation energies of propagation and deactivation. Figure 20 depicts the temperature perturbation impressed upon the system. Each perturbation lasts for about 15 min with a transition period of about 3–4 min between perturbations. The kinetic response of the system is also shown in Figure 20. The plots and least-squares estimates used to determine E_p and E_d from the experimental data are shown in Figure 20. The estimated value for the activation energy of propagation, E_p, is found to be 13.5 $\pm$ 0.62 kcal/mol, which lies very close to the expected range of 10–13 kcal/mol required for the opening of carbon–carbon double bonds.[41] The estimated value for E_d is found to be approximately 16.0 $\pm$ 0.63 kcal/mol.

Catalyst Deactivation—Copolymerization

Kinetic parameters E_p and E_d were estimated for a range of monomer compositions. The simulation results assuming first-order decay compare well with the experimental results (see Figs. 21 and 22). Figure 23 shows the linear relationship between k_d and $1/T$ on the logarithmic scale. The tabulated set of data shows that E_d lies in the range of 12.75–13.8 kcal/mol (Table III). Thus, the difference in values of E_d obtained from the different types of perturbations under the various polymerization conditions is not very significant.

Monomer Propagation—Copolymerization

The Arrhenius plots of $Rp^{\text{corr}}(T)$ versus $1/T$ for the temperature step-up, step-down, and pulse

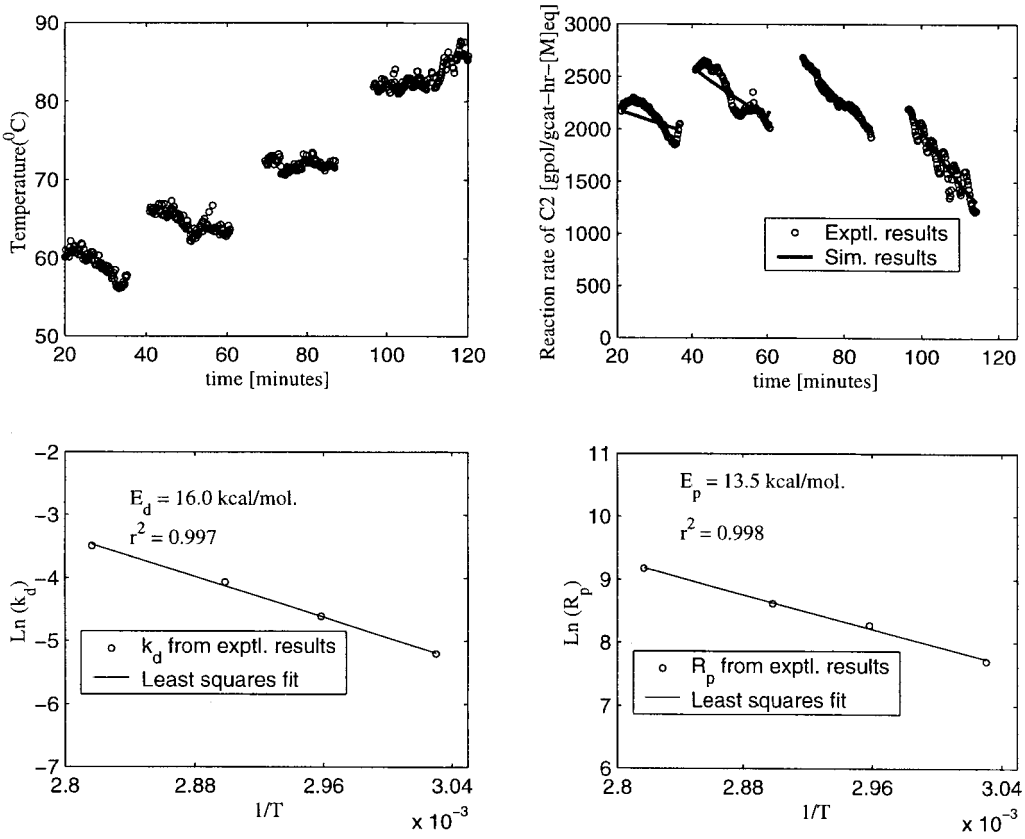

Figure 20 Perturbation results for ethylene homopolymerization.

techniques are presented in Figure 24. Theoretically, the value of E_p can be calculated from quantum chemistry because it involves a double-bond opening. According to Kissin,[41] the typical value for many catalytic reactions involving double-bond openings are usually in the range of 10–13 kcal/mol. Table IV shows that the values obtained in the study fall into this range. The estimated values are also similar to those reported by Hamba et al.[39] and Debling[26] for a classical Ziegler–Natta catalyst.

Reactivity Ratios

The effect of comonomer incorporation in this work was studied by controlling the comonomer composition. The comonomer composition in the polymer is calculated based upon the instantaneous consumption rates of ethylene and propylene. Table V summarizes the cumulative results obtained from each reaction run. The reactivity ratios can be obtained with the Fineman–Ross method:

$$\frac{F(f-1)}{f} = \frac{F^2}{f} r_1 - r_2 \tag{20}$$

where

$$F = \frac{[M_1]_{eq}}{[M_2]_{eq}}$$

$$f = \frac{\text{monomer 1 in polymer}}{\text{monomer 2 in polymer}} \tag{21}$$

Monomers 1 and 2 represent ethylene and propylene in this study, respectively. Figure 25 shows the Fineman–Ross plots obtained at 62, 70, and 80°C. The value of r_1 changes from 14.6 to 18.7, which might seem to be a significant change. However, the possible role of diffusion limitations exists in results obtained from the data collected at 80°C because of the polymer particle sintering observed. Hence, the lower-temperature values are probably more reliable.

Reaction-rate Order

Step-up and step-down perturbations in the reactor pressures (i.e., equivalent to changing the partial pressure of the monomer) are employed to determine the overall reaction rate orders of the

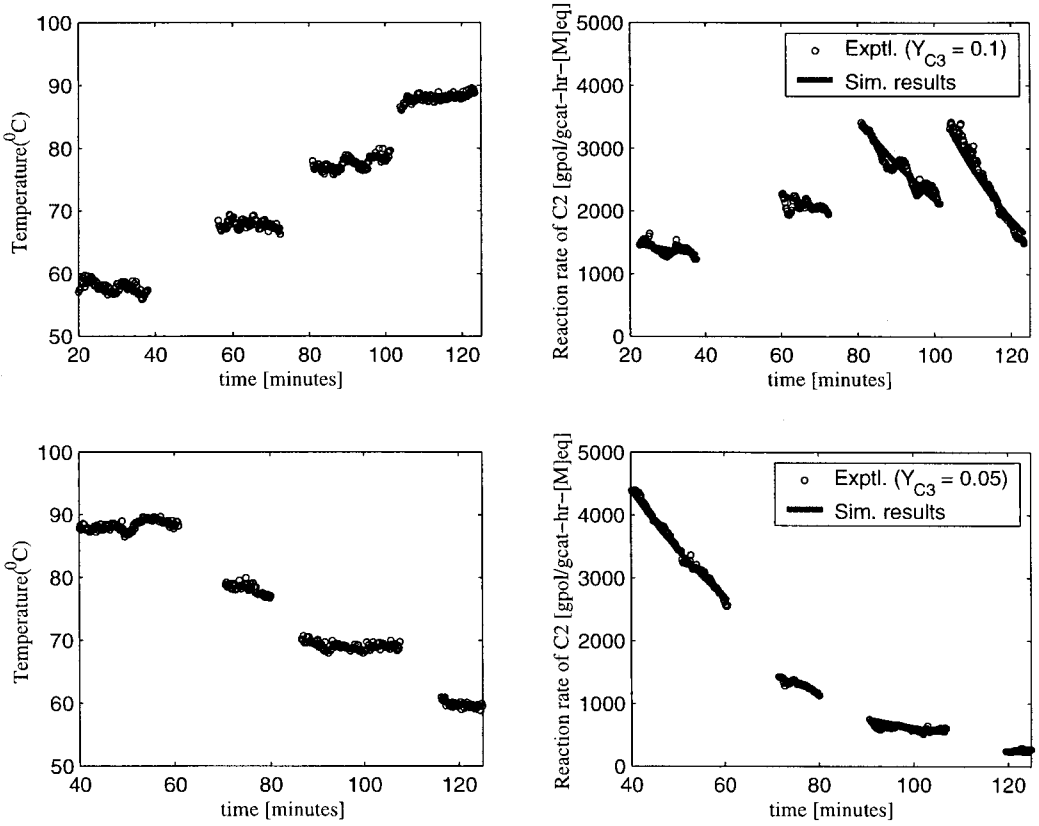

Figure 21 Perturbation results for the step-up and step-down strategies.

individual monomers. For ethylene homopolymerization, the plots of reaction rates corrected for catalyst decay are shown in Figures 26 and 27. The observed reaction-rate order is approximately 2 (see Fig. 28). Figures 29 and 30 shows the corrected reaction rates associated with changes in ethylene partial pressure in ethylene/propylene copolymerization. Close to first-order dependency is obtained for copolymerization (see Fig. 31).

Pasquet and Spitz[42] obtained a reaction-rate order of about 2.6 for ethylene homopolymerization in a slurry reactor. In the presence of an α-olefin, the reaction order of ethylene was found to be about 1.6. Karol et al.[43] found the reaction order of ethylene to be 2 for homopolymerization and 1 in the presence of an α-olefin. They attributed the reaction order departure from 1 to the monomers participating in the site activation step. Han-Adebekun[30] found that the reaction order for ethylene is around 1.6 for ethylene homopolymerization with a supported Ziegler–Natta catalyst in the gas-phase reactor system. However, propylene showed first-order kinetics when homopolymerization was conducted. Using a similar catalyst, Debling[26] observed first-order dependencies for both ethylene and propylene after propylene prepolymerization was conducted. It appears that this is the first report of the same phenomena for metallocenes.

Model Building

Ethylene Homopolymerization

- Kinetic scheme

For ethylene homopolymerization, a one-site model is proposed to predict the trends observed with changing temperatures. Table VI shows the elementary reactions which include site activation by monomer, propagation, and spontaneous catalyst deactivation.

- Parameter estimation.

The proposed kinetic scheme contains six parameters that need to be estimated. They include the preexponential factor and activation energy for the kinetic rate constant in every elementary reaction step. Using perturbation techniques pre-

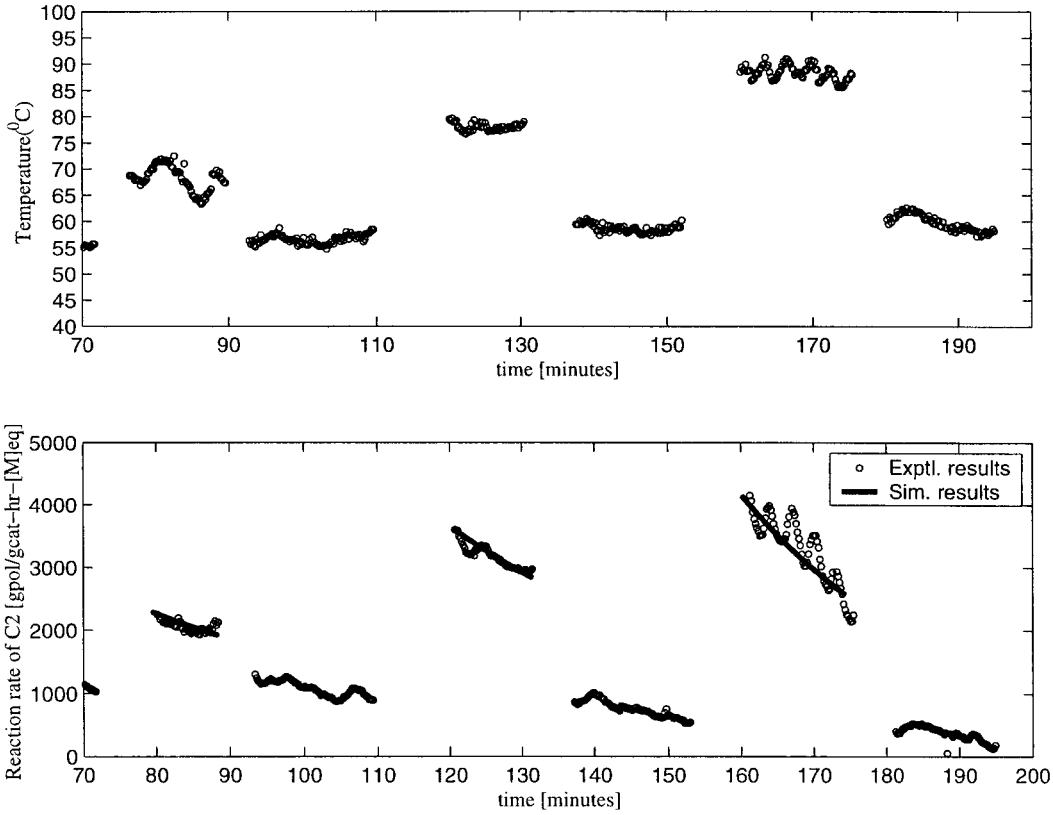

Figure 22 Comparison of the experimental and simulation results for the pulse strategy; $Y_{C3} = 0.1$.

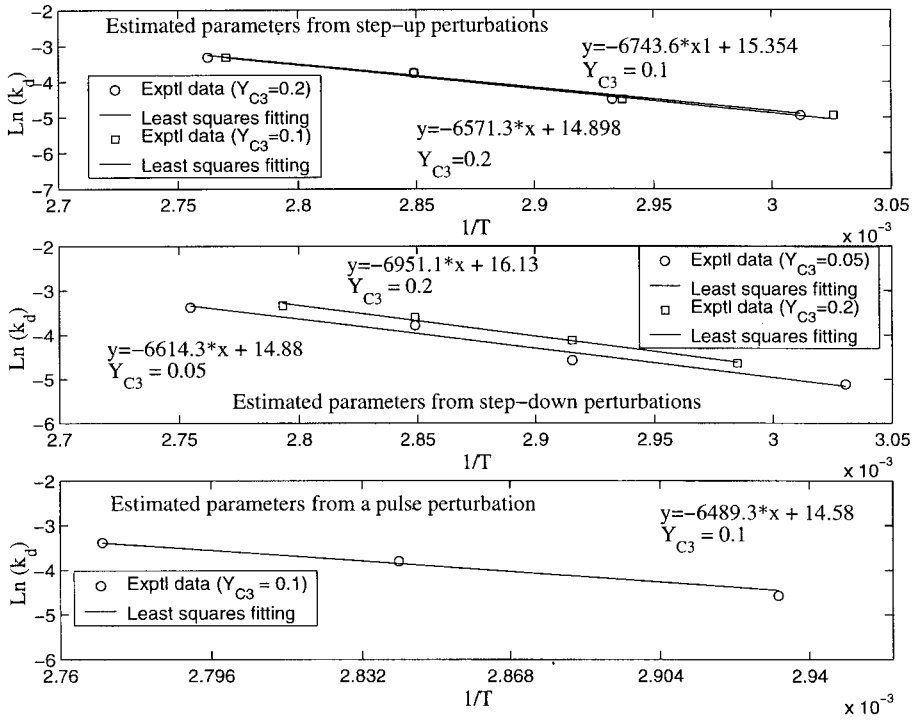

Figure 23 Arrhenius plot of k_d versus $1/T$ for the different perturbation techniques.

Table III Determination of E_d

Perturbation Type	Comonomer Concentration	E_d (kcal/mol)
Step-down	5%	13.14 ± 0.9
Step-up	20%	13.1 ± 0.94
Step-down	20%	13.8 ± 1.04
Step-up	10%	13.3 ± 1.02
Pulse	10%	12.9 ± 1.45

viously described, the activation energies of propagation and deactivation were estimated. To test the techniques for effectiveness and consistency, a dual approach was considered:

–Method 1: All the six parameters were estimated.

–Method 2: The values for the activation energies of propagation and deactivation obtained from the perturbation techniques are kept constant, while the other four parameters are estimated.

For both methods, the centering-point technique was implemented to reduce the interaction between the activation energy and the preexponential factors. This technique has proved to be more effective in estimating the two kinetic parameters simultaneously.[44,45]

The results obtained by the two methods are tabulated in Table VII. For determining the preexponential factors of site activation and propagation, the products, $k_{ao}C_{pot}$ and $k_{po}C_{pot}$ need to be divided by the exact site concentration for the catalyst. For the POLYRED simulations, the value of C_{pot} was equal to 1.25×10^{-4}. The relationship between C_{pot} and C^* is shown in Table VI. Values estimated for the activation energies of propagation and deactivation are consistent with those obtained from the perturbation techniques. This procedure corroborates the accuracy and effectiveness of the perturbation techniques. Hence, when confronted with a larger set of parameters as will be seen in copolymerization, the results from the perturbation techniques can be used to minimize the number of parameters to be estimated simultaneously.

- Model Predictions

The model predictions from the two estimation methods are quite consistent as can be seen in Figure 32. But in the case of 62 and 70°C, the model fails to capture the position of the peak. This can be attributed to the initial induction period in the experimental reaction temperature

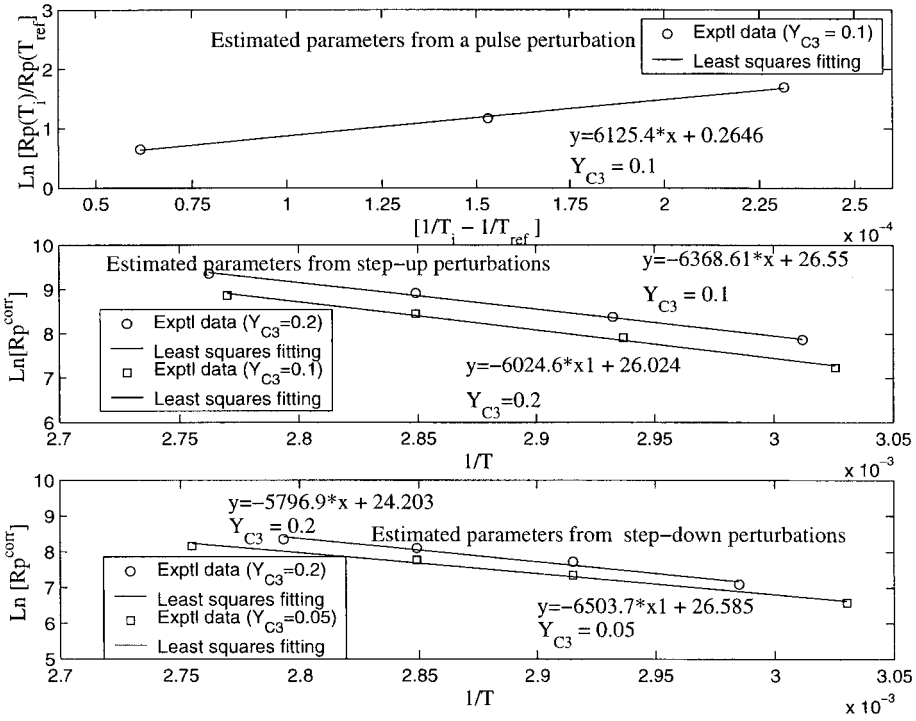

Figure 24 Arrhenius plot of k_p versus $1/T$ for the different perturbation techniques.

Table IV Determination of E_p

Perturbation Type	Comonomer Concentration	E_p (kcal/mol)
Step-down	5%	11.52 ± 1.15
Step-up	20%	11.97 ± 0.79
Step-down	20%	12.92 ± 0.51
Step-up	10%	12.60 ± 0.56
Pulse	10%	12.10 ± 0.45

profiles obtained for these conditions. This is in contrast to the simulations where it is assumed that the reaction temperature is at the set point from the onset of the reaction.

Ethylene Copolymerization

- Kinetic Scheme

For copolymerization, where there is a rate enhancement due to site activation by the α-olefin, a two-site model was proposed to explain the observed kinetics. The elementary reactions in the kinetic scheme are summarized in Table VIII. It should be noted that a single-site model failed to predict the ethylene reaction rates at the various reaction conditions. Compared to the kinetic scheme proposed for homopolymerization, the first additional reaction in this kinetic scheme involves site activation by the comonomer. This has been previously proposed by other authors[38,43] for conventional Ziegler–Natta catalysts. Also, a site-transformation reaction is proposed. This particular reaction is present in the kinetic schemes proposed by Vela Estrada and Hamielec[14] for ethylene homopolymerization and Mulhaupt et al.[16] for propylene homopolymerization. In the former, it was shown to occur at higher temperatures, while in the latter, tributylaluminum (TIBA) proved to be responsible for this reaction. This two-site kinetic scheme can be embedded into a comprehensive kinetic model which is available for transition-metal-catalyzed olefin polymerization in the polymerization modeling package POLYRED™.

- Parameter estimation from POLYRED™

Unlike ethylene homopolymerization where only six parameters had to be estimated, copolymerization presents us with the situation where a large number of parameters need to be estimated. With the effectiveness of the perturbation techniques having been proved from the ethylene homopolymerization results, average values for E_p and E_d obtained from the copolymerization perturbation methods were used in the current estimation effort.

A total of five preexponential factors need to be estimated in the proposed kinetic model for ethylene/propylene copolymerization. They are associated with the propagation of monomer 1 at both sites $k^1_{p,110}$ and $k^2_{p,110}$, site transformation from 1 to 2 due to the introduction of comonomer (propylene) $k^{1\to2}_{\mathrm{tr},0}$, and deactivation at both sites $k^1_{d,0}$ and $k^2_{d,0}$. All the parameters are multiplied by C_{pot} since the exact site concentration for the catalyst is not known. The value used in the sim-

Table V Propylene Composition in the Polymer

Sample	Temperature (°C)	C3 in Gas (m.f.)	C3 Sorbed (m.f.)	C3 in Polymer (m.f.)
EP-05P-62C	62	0.05	0.15	0.012
EP-10P-62C	62	0.10	0.27	0.023
EP-20P-62C	62	0.20	0.45	0.045
EP-30P-62C	62	0.30	0.58	0.105
EP-05P-70C	70	0.05	0.14	0.011
EP-10P-70C	70	0.10	0.25	0.035
EP-20P-70C	70	0.20	0.44	0.040
EP-30P-70C	70	0.30	0.57	0.119
EP-05P-80C	80	0.05	0.13	0.009
EP-10P-80C	80	0.10	0.24	0.021
EP-20P-80C	80	0.20	0.42	0.045
EP-30P-80C	80	0.30	0.55	0.051

m.f.: mol fraction.

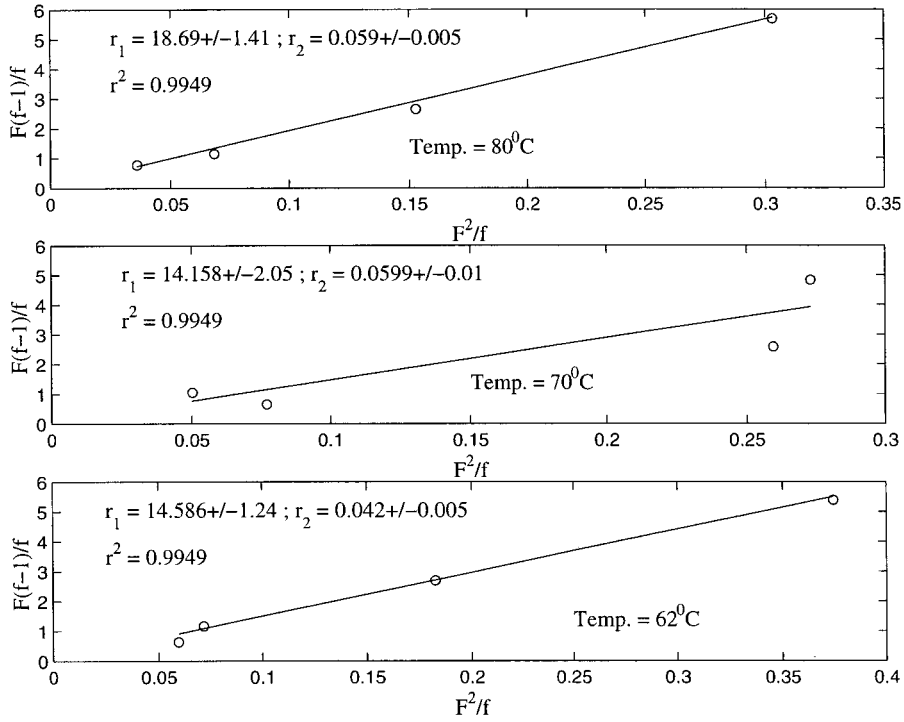

Figure 25 Reactivity ratios obtained at different temperatures.

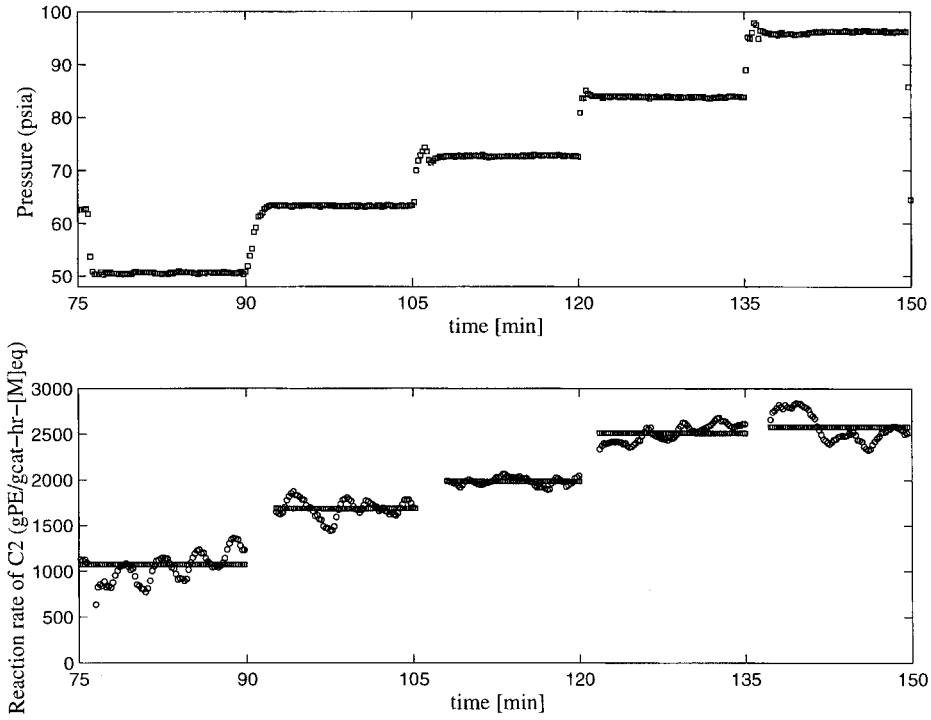

Figure 26 Pressure perturbations in ethylene homopolymerization; corrected for catalyst decay: step-up.

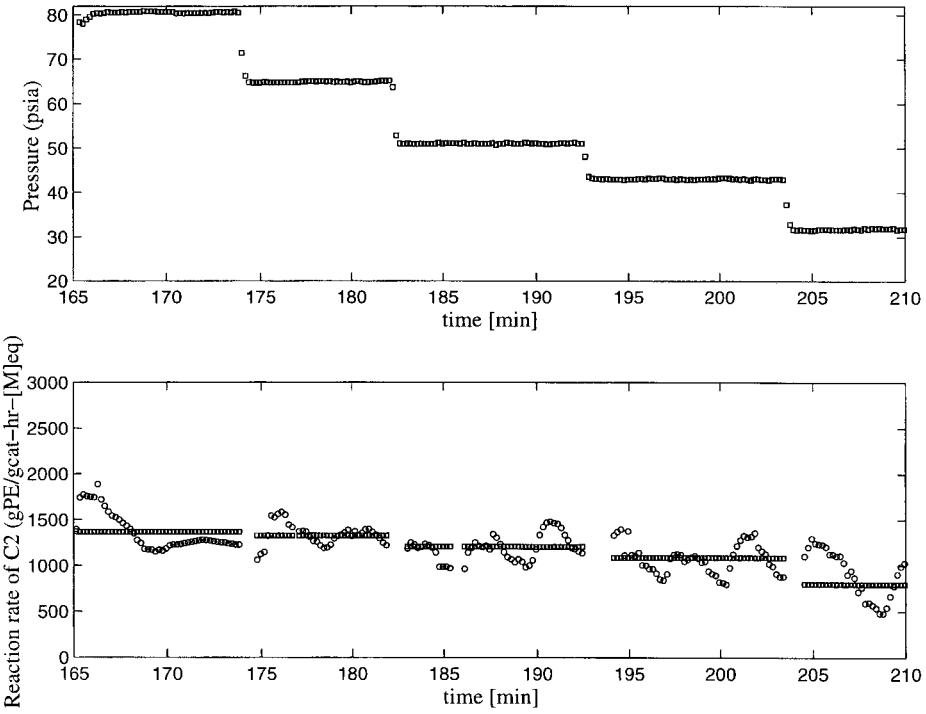

Figure 27 Pressure perturbations in ethylene homopolymerization; corrected for catalyst decay: step-down.

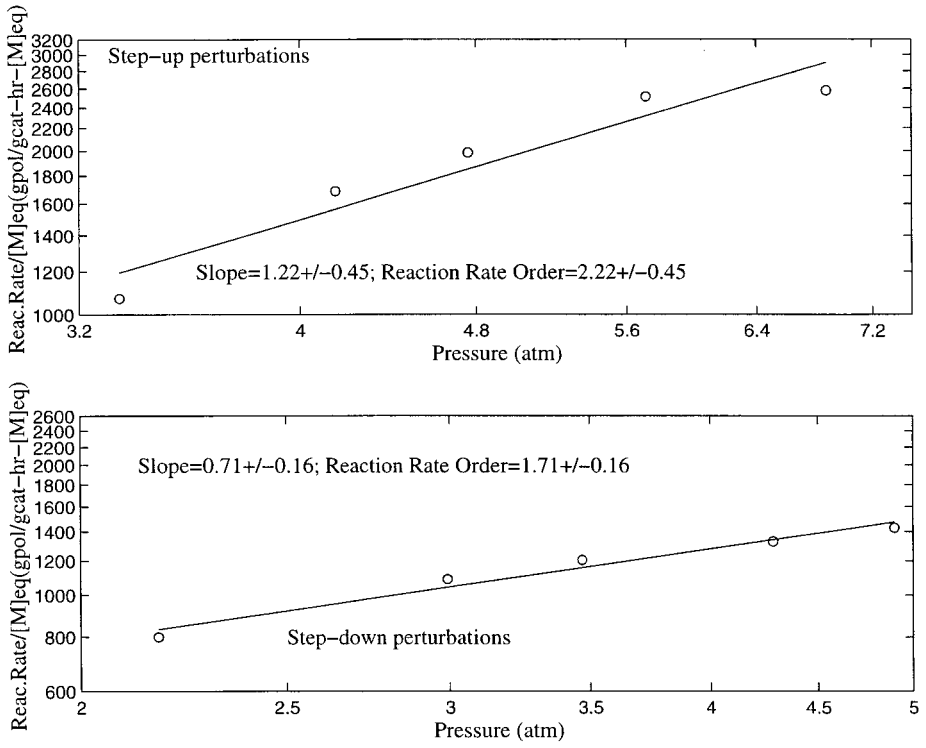

Figure 28 Determination of reaction-rate order for ethylene homopolymerization.

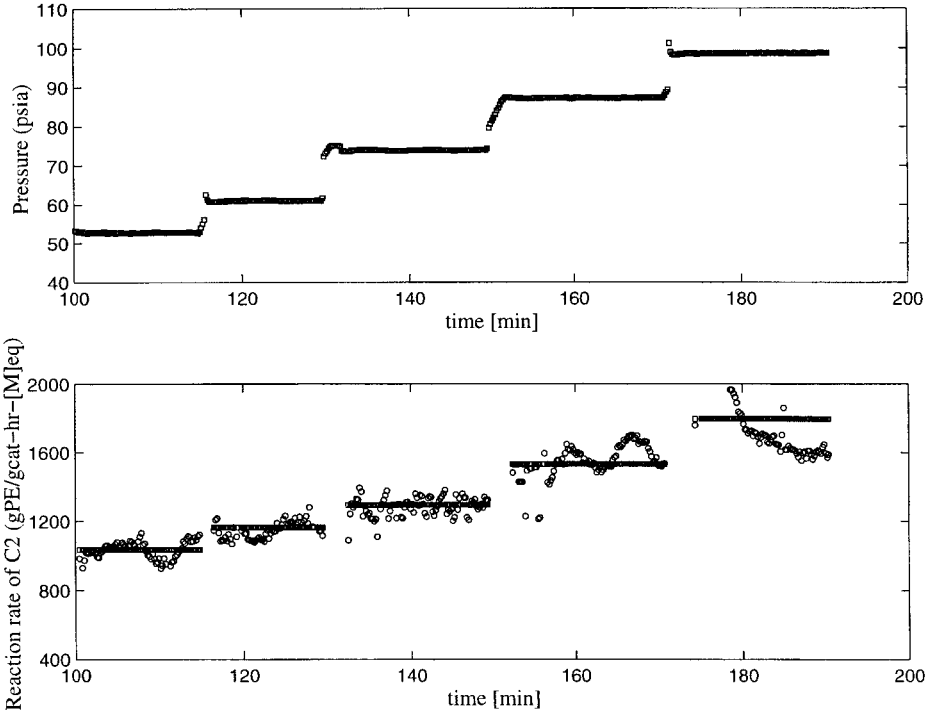

Figure 29 Pressure perturbations in ethylene copolymerization; corrected for catalyst decay: step-up.

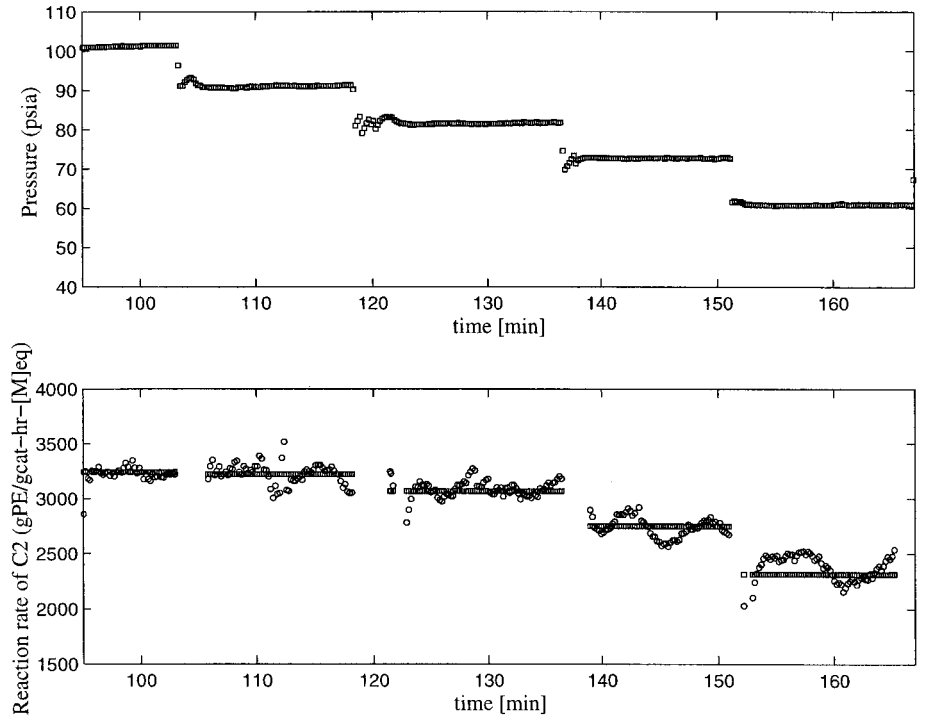

Figure 30 Pressure perturbations in ethylene copolymerization; corrected for catalyst decay: step-down.

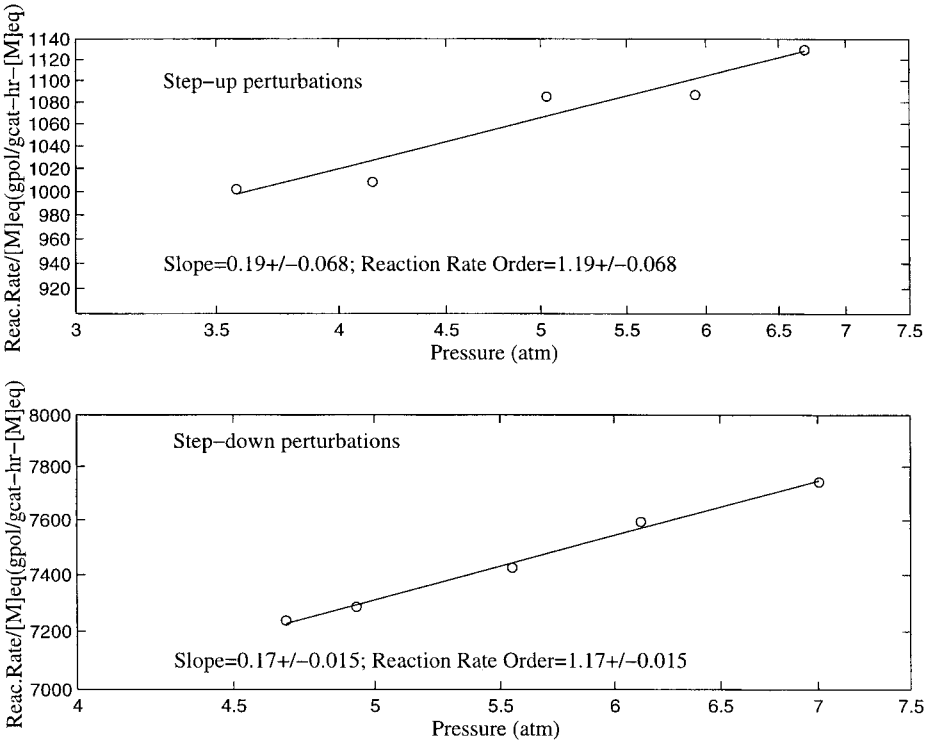

Figure 31 Determination of reaction-rate order for ethylene copolymerization.

ulations was 1.67×10^{-4}. The relationship between C_{pot} and C^* is provided in Table VIII. In addition, the activation energy of site transformation is estimated. The centering-point technique was implemented in estimating the necessary parameters. The parameters not included in the estimation are the kinetic rate constants of activation of site 1 by the two monomers and the propagation rate constants for propylene at both the sites. When it was found that the values failed to change during estimation calculations, they were excluded from the set of parameters being estimated. Apparently, the default values are adequate to represent the experimental data. In terms of sensitivity, it is important to note that while changes in these parameters of a factor of 2–3 does not affect the model prediction large changes of an order of magnitude of the default parameters associated with cross propagation or site activation will alter model predictions. Since the activation energy of propagation for the two monomers was the same, the reactivity ratios obtained are a ratio of the preexponential factors of the propagation rate constants. Hence, they are independent of temperature. Table IX shows the values obtained for the reactivity ratios following the estimation of the preexponential factors.

Table VI Elementary One-site Reaction-rate Model for Homopolymerization

Name	Reaction
Activation	$C_{\text{pot}} + M \rightarrow C_o^*$
Propagation	$C_n^* + M \rightarrow C_{n+1}^*$
Deactivation	$C_n^* \rightarrow C_d + D_n$

Determination of the number of experiments to be employed for parameter estimation is not a trivial task. In principle, all the copolymerization experiments could be used to perform parameter estimation. However, the current reactor model in POLYRED™ assumes that there is no monomer diffusion limitation. For the experiments performed at high reaction temperatures (80°C) and high comonomer compositions (30 mol %), the polymer obtained was found to be more sticky compared to the other runs. Possible reasons include polymer partially melting which would cause monomer diffusion limitations. Hence, the current model would not prove to be appropriate in describing the reaction kinetics for these conditions. A set of experiments where it is suspected that monomer diffusion and the other confound-

Table VII Kinetic Parameters for Homopolymerization

Parameter	Estimated Value		Units
	Method 1	Method 2	
	Preexponential Factors		
Site activation, $k_{ao}C_{pot}$	0.74×10^{1}	1.20×10^{1}	(cc-amor.poly./gCat s)
Propagation, $k_{po}C_{pot}$	1.5×10^{10}	1.03×10^{10}	(cc-amor.poly./gCat s)
Deactivation, k_{do}	1.9×10^{7}	1.1×10^{7}	s^{-1}
	Activation Energies		
Site activation, E_a	4.54	4.88	kcal/mol
Propagation, E_p	13.87	13.5[a]	kcal/mol
Deactivation, E_d	16.90	16.0[a]	kcal/mol

[a] Estimated via online perturbation.

ing factors will not have a significant impact on the ethylene reaction rates are used to estimate parameters. After careful examination, seven sets of data (EP-5P-62C, EP-10P-62C, EP-20P-62C, EP-5P-70C, EP-10P-70C, EP-20P-70C, and EP-5P-80C) were used in our kinetic parameter estimation. The results obtained were then used to predict the kinetics under the other reaction conditions not included in the parameter estimation. The estimated kinetic parameters from POLYRED™, together with those estimated via online perturbation, are summarized in Table IX. To estimate the preexponential factors for activation, propagation, and deactivation, the exact active-site concentration for the catalyst needs to be known.

The difference observed in the values obtained for the reactivity ratios can be explained by studying Figures 33 and 34. The data used in determining the reactivity ratios in Figure 25 are based on the cumulative yield obtained from several different runs. Figure 33 illustrates the observed increase in the instantaneous ethylene weight fraction in the polymer over the course of an individual run and the corresponding increase in the instantaneous value of r_1 is shown in Figure 34. Here, r_1 is calculated using a simplified form of the Mayo equation[46,47]:

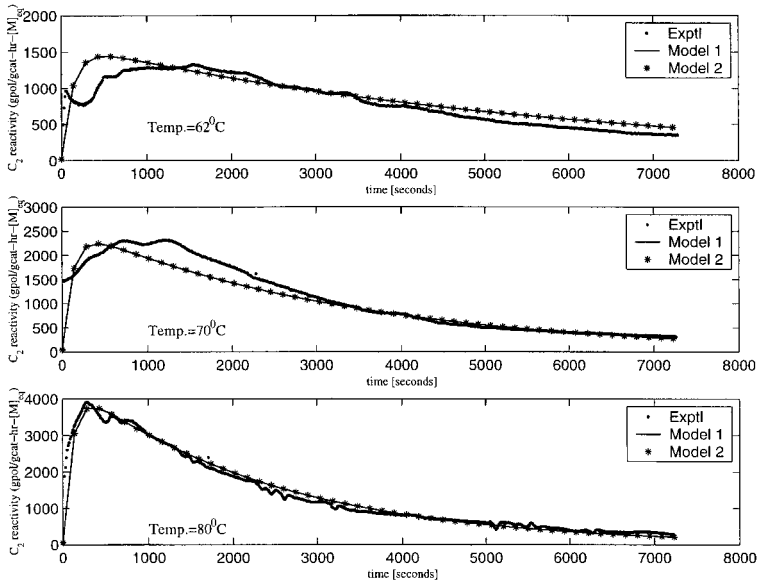

Figure 32 Comparison between experimental and modeling results from the two-parameter estimation strategies at 62, 70, and 80°C.

Table VIII Elementary Two-site Reaction-rate Model for Ethylene/Propylene Copolymerization

Name	Reaction
Activation	$C_{pot} + M_i \rightarrow C^{*,1}_i$
Propagation	$C^{*,k}_i + M_j \rightarrow C^{*,k}_j$
Deactivation	$C^{*,k}_i \rightarrow C_d + D^k_n$
Site transformation	$C^{*,1} + M_2 \rightarrow C^{*,2}$

k = 1 or 2; i = monomer 1 or 2.

$$\left(\frac{M_2}{M_1}\right)_{polymer} = \frac{1}{r_1}\left(\frac{M_2}{M_1}\right)_{sorb} \quad (22)$$

where M_2 and M_1 are propylene and ethylene, respectively. This increase in the value of r_1 (in Fig. 34) is represented by a larger value for r_1 for the second site in Table IX. The rate at which the second site is formed increases at higher temperatures and higher comonomer compositions; hence, a smaller change in the value of r_1 over the reaction time would be expected (shown for 80°C in Fig. 34). Finally, note that the set of kinetic parameters estimated here is by no means a unique set. However, they are physically plausible and do represent the data well.

- Model Prediction

Figures 35–38 show the model predictions and ethylene reaction rates obtained from the ethylene–propylene copolymerization experiments. It is seen that the reaction rates predicted from the model provide a reasonable fit and capture the trends observed in the experiments at 62 and 70°C.

Using the estimated kinetic parameters in Table IX, the ethylene reaction rates under the other reaction conditions not used in the parameter estimation can be simulated. The model predicts higher reaction rates at a temperature of 80°C than those observed from experiments when the propylene composition is above 5% (mol) in the gas phase (see Figs. 36–38).

According to Hamba et al.,[39] the transition temperature at which polymer sintering leads to the destruction of polymer particle pores and the onset of monomer diffusion limitation changes with the copolymer composition. Based upon their

Table IX Kinetic Parameters for Copolymerization

Parameter	Estimated Value: Site 1	Estimated Value: Site 2	Units
	Preexponential Factors		
Site activation, $k_{ao,1}C_{pot}$ [a]	2.01×10^3	—	(cc-amor.polymer/gCat s)
Site activation, $k_{ao,2}C_{pot}$ [a]	3.01×10^2	—	(cc-amor.polymer/gCat s)
Propagation, $k_{po,11}C_{pot}$ [b]	2.06×10^9	5.11×10^{10}	(cc-amor.polymer/gCat s)
Propagation, $k_{po,12}C_{pot}$ [a]	1.32×10^8	2.72×10^9	(cc-amor.polymer/gCat s)
Propagation, $k_{po,21}C_{pot}$ [a]	3.0×10^8	9.02×10^8	(cc-amor.polymer/gCat s)
Propagation, $k_{po,22}C_{pot}$ [a]	9.19×10^6	2.67×10^7	(cc-amor.polymer/gCat s)
Site transformation, $k^{1\rightarrow 2}_{tro}C_{pot}$ [b]	3.01×10^1	—	(cc-amor.polymer/gCat s)
Deactivation, k_{do} [b]	1.81×10^4	7.84×10^5	s^{-1}
	Activation Energies		
Site activation, E_a [a]	10.0	10.0	kcal/mol
Propagation, E_p [c]	12.0	12.0	kcal/mol
Site transformation, $E_{tr_{S1\rightarrow S2}}$ [b]	7.7	—	kcal/mol
Deactivation, E_d [c]	12.9	12.9	kcal/mol
	Reactivity Ratios		
r_1	15.54	18.71	—
r_2	0.03	0.03	—

[a] Default value in POLYRED™.
[b] Estimated Using POLYRED™.
[c] Estimated via online perturbation.

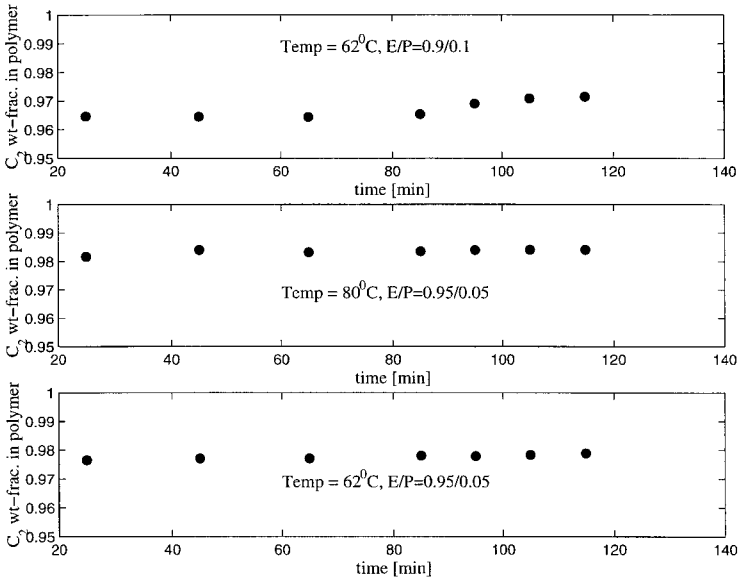

Figure 33 Change in the weight fraction of ethylene in the polymer versus reaction time.

experiments with a supported $TiCl_4$ catalyst, they found the transition temperature to be 93°C for ethylene homopolymerization and 74°C for ethylene/propylene copolymerization with 25% (mol) of propylene in the gas phase. These temperatures could be lower in this study because a supported metallocene catalyst was used. It is reported that the melting point of the polymer produced using metallocene catalysts is often 10 or 15°C lower than that produced with the supported conventional Ziegler–Natta catalysts.[48] Thus, as the comonomer content increases, the metallocene

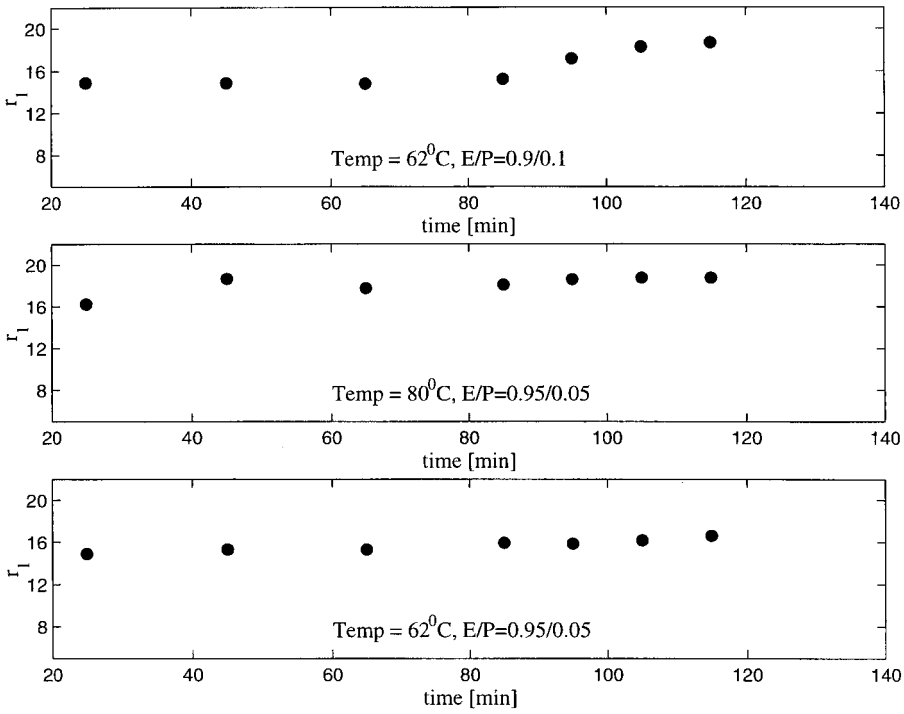

Figure 34 r_1 versus reaction time.

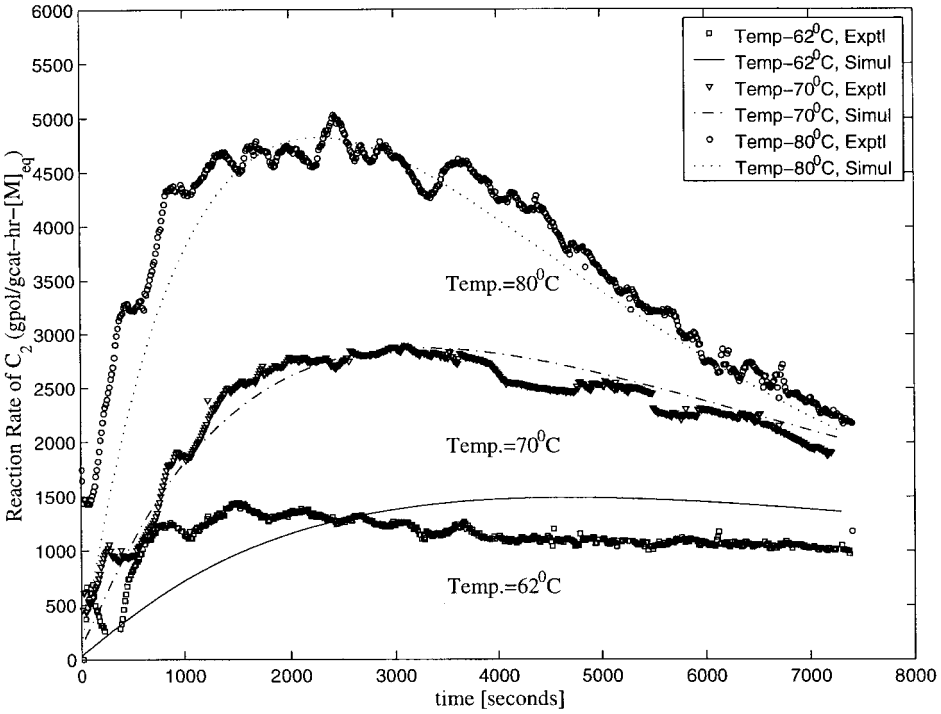

Figure 35 Comparison between experimental and simulation results for ethylene copolymerization with 5% propylene in the gas phase.

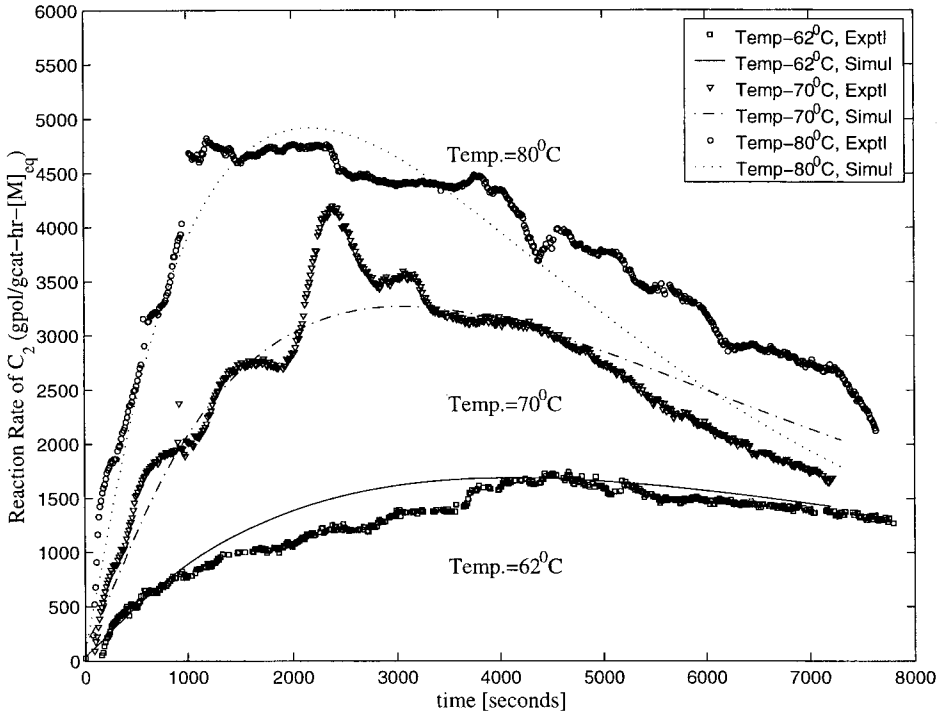

Figure 36 Comparison between experimental and simulation results for ethylene copolymerization with 10% propylene in the gas phase.

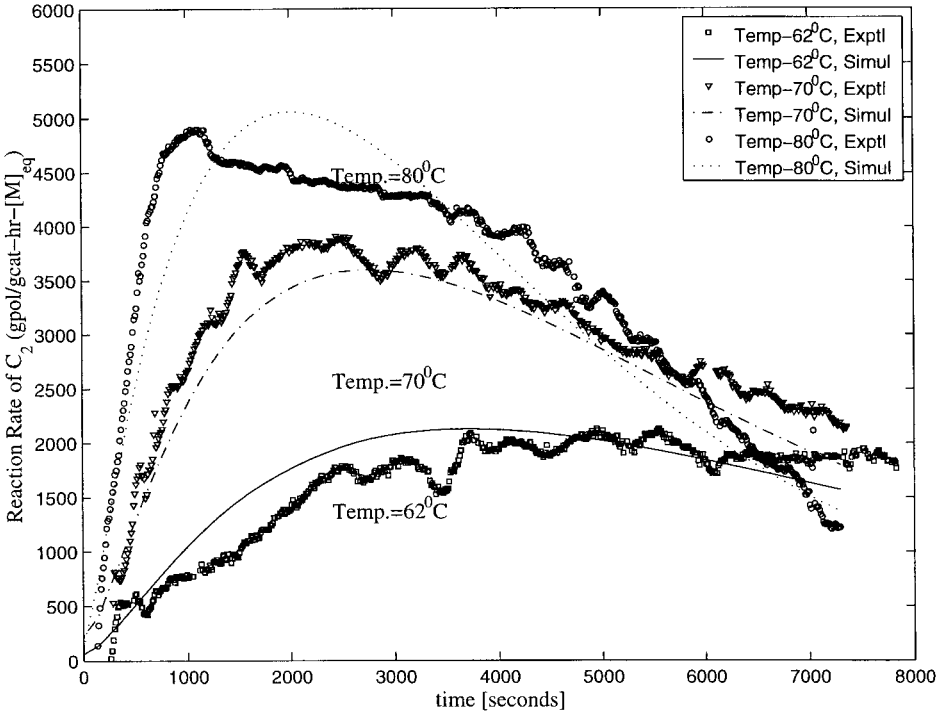

Figure 37 Comparison between experimental and simulation results for ethylene copolymerization with 20% propylene in the gas phase.

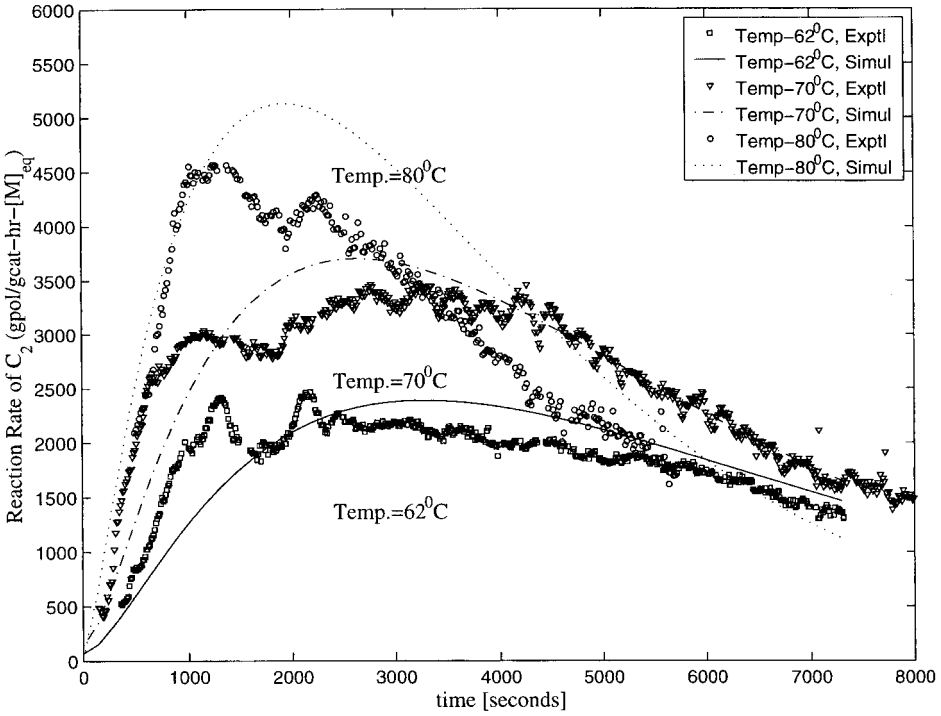

Figure 38 Comparison between experimental and simulation results for ethylene copolymerization with 30% propylene in the gas phase.

polymer formed has a lower crystallinity, indicating that the softening point of the polymer will be lower. This implies that a copolymerization conducted at 80°C with a higher propylene content (10–30%) could have already crossed the transition temperature and that diffusion limitations could have reduced the intrinsic reaction rates.

CONCLUSIONS

The kinetics of supported metallocene-catalyzed ethylene homopolymerization and ethylene–propylene copolymerization were studied in a gas-phase reactor system. An experimental procedure was developed, by which it was possible to obtain reproducible and consistent data. First, the influence of temperature on ethylene homopolymerization was investigated. Then, both temperature and comonomer effects on the kinetics of ethylene–propylene copolymerization were studied. With increasing temperatures, the magnitude of the reaction rate peak increased for both homopolymerization and copolymerization. The presence of the comonomer had a positive effect on the intrinsic reaction rate of ethylene. Temperature and pressure perturbation techniques were implemented to determine activation energies and reaction-rate orders, respectively. A single-site model proved to be adequate in explaining the trends observed for ethylene homopolymerization. For copolymerization, a two-site model was instituted to explain the comonomer and temperature effects observed. The model, however, failed to predict the kinetics for copolymerization at 80°C for higher concentrations of propylene. This was attributed to the model not taking into account polymer particle sintering with resulting monomer diffusion which becomes an important factor at higher temperatures.[25]

The experimental and parameter estimation procedures developed here have been shown to be effective in creating a kinetic model for supported metallocene catalysts. The results from perturbation methods have proved to be consistent, thereby facilitating estimation of E_p, E_d, and the reaction-rate order. The Fineman–Ross method provided a reasonable estimate for the reactivity ratios and a good starting point for further estimation of the cross-propagation constants. Preexponential factors and activation energies for the other reactions in the kinetic scheme were estimated, but were not uniquely determined since the problem was confounded by a large set of parameters. The model is able to represent well the kinetics of the catalyst system for ethylene homo- and copolymerization.

The authors would like to thank Dr. S. X. Zhang and Dr. J. Brinen from Exxon for useful technical discussions.

REFERENCES

1. Brinen, J. L.; Muhle, M. E. In Polymer Reaction Engineering III, Engineering Foundation, New York, 1997.
2. Soares, J. B. P.; Hamielec, A. E. Polym React Eng 1995, 3, 131–200.
3. Brockmeier, N. F.; Koizumi, T. In Reactor Engineering Conference, 1991.
4. Sinclair, K. B. Annual Meeting of the American Institute of Chemical Engineers, [Preprints] New York, 1985.
5. Tait, P. J. T. Trans Met Init Rel Polym 1986, 49(13), 1–25.
6. Hamielec, A. E.; Soares, J. B. P. Polym React Eng 1995, 3, 439–514.
7. Hamielec, A. E.; Soares, J. B. P. Prog Polym Sci 1996, 21, 651–706.
8. Chien, J. C. W. In MetCon′93, 1993.
9. Gupta, V. K.; Satish, S.; Bhardwaj, I. S. JMS-Rev Macromol Chem Phys 1995, 34, 439–514.
10. Kaminsky, W. Catal Today 1994, 20, 257–271.
11. Kashiwa, N.; Todo, A. In MetCon′93, Mitsui Petrochemical Industries Ltd, 1993.
12. Huang, J.; Rempel, G. L. Prog Polym Sci 1995, 20, 459–526.
13. Reddy, S. S.; Sivaram, S. Prog Polym Sci 1995, 20, 309–367.
14. Vela Estrada, J. M.; Hamielec, A. E. Polymer 1994, 808, 34–44.
15. Bonini, F.; Fraaije, V.; Fink, G. J Polym Sci Part A Polym Chem 1994, 40, 1–14.
16. Jungling, S.; Koltzenburg, S.; Mulhaupt, R. J Polym Sci Polym Chem 1997, 35, 1–8.
17. Chien, J. C. W.; He, D. J Polym Sci Part A Polym Chem 1991, 29, 1585–1593.
18. Chien, J. C. W.; He, D. J Polym Sci Part A Polym Chem 1991, 29, 1595–1601.
19. Chien, J. C. W.; He, D. J Polym Sci Part A Polym Chem 1991, 29, 1603–1607.
20. Tsutsui, T.; Kashiwa, N. J Polym Sci Part A Polym Chem 1994, 34, 439–514.
21. Chien, J. C. W.; Yu, Z.; Marques, M. M.; Flores, J. C.; Rausch, M. D. J Polym Sci Part A Polym Chem 1998, 36, 319–328.
22. Kravchenko, R.; Waymouth, R. M. Macromolecules 1998, 31, 1–6.
23. Tsutsui, T.; Kashiwa, N. Polymer 1991, 32, 2671–2673.
24. Ray, W. H. In Transition Metal Catalyzed Polymerizations, Quirk, R. P., ed. Cambridge University Press, New York, p. 563; 1988.

25. Han-Adebekun, G. C.; Hamba, M.; Ray, W. H. J Polym Sci Part A Polym Chem 1997, 35, 2063–2074.
26. Debling, J. A. PhD Thesis, University of Wisconsin, 1997.
27. Choi, K.-Y. PhD Thesis, University of Wisconsin, 1984.
28. Chen, C. M. PhD Thesis, University of Wisconsin, 1993.
29. Han-Adebekun, G. C.; Debling, J. A.; Ray, W. H. J Appl Polym Sci 1997, 64, 373–382.
30. Han-Adebekun, G. C. PhD Thesis, University of Wisconsin, 1996.
31. Ogunnaike, B. A.; Ray, W. H. Process Dynamics, Modeling and Control; Oxford University: New York, 1994.
32. Keii, T. Kinetics of Ziegler–Natta Polymerization; Kodansha: Tokyo, Japan, 1972.
33. Ewen, J. A.; Elder, M. J. Macromol Chem Macromol Symp 1993, 66, 179–190.
34. Chakravarti, S. Master's Thesis, University of Wisconsin, 1997.
35. Chien, J. C. W.; Wang, B.-P. J Polym Sci Part A Polym Chem 1990, 28, 15–38.
36. Chien, J. C. W.; Razavi, A. J Polym Sci Part A Polym Chem 1988, 26, 2369–2380.
37. Eskelinen, M.; Seppala, J. V. Eur Polym J 1996, 32, 331–335.
38. Pasquet, V.; Spitz, R.; Gomez, C.; Guyot, A. In Proceedings of ACS, Division of Polymeric Materials; Science and Engineering, 1992; pp 59–60.
39. Hamba, M.; Han-Adebekun, G. C.; Ray, W. H. J Polym Sci Part A Polym Chem 1997, 35, 2075–2096.
40. Stein, S. A.; Mulhaupt, J. T.; Garies, P. J. AIChE J 1969, 15, 64.
41. Kissin, Y. V. Isospecific Polymerization of Olefins with Heterogeneous Ziegler–Natta Catalysts; Springer-Verlag: New York, 1987.
42. Pasquet, V.; Spitz, R. Makromol Chem 1993, 94, 451–461.
43. Karol, F. J.; Kao, S.; Cann, K. J. J Polym Sci Part A Polym Chem 1993, 31, 2541–2553.
44. Pritchard, D. J.; Bacon, D. W. Chem Eng Sci 1975, 30, 567–574.
45. Box, G. E. P. Ann NY Acad Sci 1960, 83, 792–816.
46. Bukatov, G. D.; Yechevskaya, L. G.; Zakharov, V. A. In Transition Metals and Organometallics as Catalysts for Olefin Polymerization, Kaminsky, W. and Sinn, eds. Springer Verlag, Berlin, p. 101; 1988.
47. Hutchinson, R. A.; Ray, W. H. J App Polym Sci 1990, 41, 51–81.
48. Bidell, W.; Fisher, D.; Hingmann, R.; Jones, P.; Langhauser, F.; Gregorius, H.; Marczinke, B. In MetCon′96, 1996.